

1 **Measurement Report: Optical Characterization, Seasonality, and Sources of**
2 **Brown Carbon in Fine Aerosols from Tianjin, North China: Year-round**
3 **Observations**

4 **Zhichao Dong¹, Chandra Mouli Pavuluri^{1*}, Peisen Li¹, Zhanjie Xu¹, Junjun Deng¹, Xueyan**
5 **Zhao¹, Xiaomai Zhao¹, Pingqing Fu¹, Cong-Qiang Liu¹**

6 ¹Institute of Surface-Earth System Science, School of Earth System Science, Tianjin University,
7 Tianjin 300072, China

8 *Correspondence to:* Chandra Mouli Pavuluri (cmpavuluri@tju.edu.cn)

9 **Abstract**

10 To investigate the optical characteristics and sources of brown carbon (BrC) in North China, where
11 the atmospheric aerosol loadings are high and have severe impacts on the Earth's climate system,
12 we collected fine aerosols (PM_{2.5}) at an urban site in Tianjin over a 1-year period. We measured
13 the ultraviolet (UV) light absorption and excitation emission matrix (EEM) fluorescence of the
14 water-soluble BrC (WSBrC) and the water-insoluble but methanol-soluble BrC (WI-MSBrC) in
15 the PM_{2.5} using a three-dimensional fluorescence spectrometer. Average light absorption
16 efficiency of both WSBrC (Abs_{365, WSBrC}) and WI-MSBrC (Abs_{365, WI-MSBrC}) at 365 nm was found
17 to be highest in winter (10.4±6.76 Mm⁻¹ and 10.0±5.13 Mm⁻¹, respectively) and distinct from
18 season to season. Averages of fluorescence index (FI) and biological index (BIX) of WSBrC were
19 lower in summer than in other seasons and opposite to that of humification index (HIX), which
20 implied that the secondary formation and further chemical processing of aerosols were intensive
21 during the summer period than in other seasons. Whereas in winter, the higher HIX together with
22 the higher FI and BIX of WI-MSBrC suggested that the BrC loading was mainly influenced by
23 primary emissions from biomass burning and coal combustion. Based on EEM, the types of
24 fluorophores in WSBrC were divided into humic-like substances (HULIS), including low-
25 oxygenated and high-oxygenated species, and protein like compounds (PLOM), whereas mostly
26 PLOM in the WI-MSBrC. The direct radiation absorption by both WSBrC and WI-MSBrC in the
27 range of 300–400 nm was accounted for ~40% to that (SFE_{Abs}, 4.97±2.71 Wg⁻¹ and 7.58±5.75 Wg⁻¹,
28 respectively) in the range, 300–700 nm.

29
30 **1 Introduction**

31 Brown carbon (BrC) is a part of organic aerosol (OA) and can absorb solar radiation in the near-
32 ultraviolet (UV) to visible (Vis) light, ranging from 300-500 nm (Liu et al., 2013). It has been well
33 recognized that BrC has a significant effect on radiative forcing at both regional and global scales
34 (Feng et al., 2013; Jo et al., 2016; Park et al., 2010). *For example*, the warming effect of water-
35 soluble BrC in the Arctic has been reported to be accounted for ~30% of that exerted by the black
36 carbon (Yue et al., 2022). The BrC not only affects the direct radiative forcing, but also has a
37 potential impact on indirect radiative forcing due to its hydrophilicity, which influences the
38 formation of cloud condensation nuclei (CCN) (Andreae and Gelencs'er, 2006; Laskin et al.,
39 2015b). In addition, BrC is mostly composed of highly conjugated aromatic ring compounds such

40 as a polycyclic aromatic hydrocarbons and high molecular weight substances with a polar
41 functional group that consists of nitrogen and/or oxygen, or humic-like substances (HULIS), which
42 could pose a risk to human health. *For example*, carbon-containing aromatic compounds can cause
43 physical weakness, decreased immunity, arteriosclerosis, etc., which will increase the mortality
44 due to cardiovascular and cerebrovascular diseases and a variety of cancers such as skin cancer,
45 pharyngeal cancer and nasal cancer (Diggs et al., 2011; Peters et al., 2008; Hecobian et al., 2010).

46 BrC can be emitted directly from primary sources such as biomass burning (Hoffer et al.,
47 2006; Brown et al., 2021), fossil fuel combustion (Jo et al., 2016), and non-combustion processes
48 such as bioaerosols (plant debris and fungi) and soil humus (Lin et al., 2014; Rizzo et al.,
49 2013; Rizzo et al., 2011). On the other hand, BrC can also be produced from complex chemical
50 reactions of volatile organic compounds (VOCs) emitted from both anthropogenic and biological
51 origin in gas-phase as well as by multiphase reactions between the gaseous, particulate and
52 aqueous constituents (Kasthuriarachchi et al., 2020; Li et al., 2020a; Laskin et al., 2015a).

53 In recent times, after establishing the fact that BrC absorb the light, the researchers are paying
54 lot of attention to measure the physical (optical) and chemical characteristics of the BrC and
55 estimate its climatic effects (Yue et al., 2019; Choudhary et al., 2021; Hecobian et al., 2010).
56 However, studies on BrC are still very limited due to difficulties in quantitative measurement of
57 light-absorbing organic components (Corbin et al., 2019; Wang et al., 2022b). In fact, based on the
58 disparity in wavelength dependence between BC and BrC, traditional optical instruments can be
59 used to obtain the BrC absorption value, but the availability of such instruments are limited, which
60 can accurately and directly differentiate the light absorption caused by the BC and BrC. On the
61 other hand, the molecular composition and optical properties of BrC are significantly changed
62 when the BrC is subjected for physical and photo-chemical processing (aging) in the atmosphere.
63 That is why, the indirect approaches have been developed to explore the molecular composition
64 including chromophores and sources of BrC through its light absorption and fluorescence
65 characteristics.

66 UV-Vis spectroscopy and excitation emission matrix (EEM) fluorescence spectroscopy are
67 considered to be common techniques for studying the optical absorption and fluorescence
68 chromophore optical and structural characteristics of complex organic materials, because each
69 chromophore has its own specific excitation-emission peak in the EEM maps (Chen et al.,
70 2016b; Coble, 2007). In recent years, combined spectrophotometric measurement and chemical
71 analysis has been applied to study the BrC in Xi'an, Northwest China (Huang et al., 2018). In fact,
72 EEM fluorescence spectroscopy provides multiple superposed spectral data. By using parallel
73 factor (PARAFAC) analysis of such spectral data, the type of chromophores can be identified and
74 their types are quantified semi-quantitatively based on the range of excitation-emission
75 wavelengths (Cao et al., 2022; Zhan et al., 2022; Murphy et al., 2013). The composition of humic-
76 like and protein-like components have been identified from the analysis of chromophores of
77 dissolved organic substances in aquatic environments (Xie et al., 2020). The fluorescence
78 technique has been widely applied to measure organics in terrestrial and oceanic systems (Murphy
79 et al., 2013; Yu et al., 2015), but has rarely been used in the study of atmospheric aerosols. Now,
80 the application of fluorescence technique has been well established in studying the molecular
81 composition of aerosols as well, the studies on identification of chromophores and thus the
82 molecular composition of BrC in the atmospheric aerosols are still very limited (Wu et al.,
83 2021a; Deng et al., 2022; Li et al., 2022; Cao et al., 2022).

84 Therefore, much attention need to be paid further, particularly on long-term and continuous
85 measurements of the optical characteristics of water-soluble BrC (WSBrC) and their temporal and

86 spatial variations. Moreover, the investigation of light absorption and fluorescence characteristics
87 of water-insoluble BrC (WIBrC) that can be extracted into a solvent with higher extraction
88 efficiency is necessary to better understand the impact of the BrC on climate change (Corbin et al.,
89 2019). In fact, such studies are very scarce, because the selection of solvents and determination of
90 extraction efficiency are difficult, although different polar chromophores could be extracted by
91 solvent extraction according to the polarity of solvent and methanol has been used as a common
92 solvent (Chen et al., 2016a). Hence, the comprehensive study of the optical properties of WSBBrC
93 and WIBrC is highly necessary to better understand the types of chromophores and optical
94 properties of atmospheric aerosols, as well as the processes of oxidation and transformations of
95 chromophores at different locale over the world.

96 China is one of the most polluted areas in the world, and suffering from the absorption and
97 scattering of solar radiation by atmospheric aerosols that directly affect the energy balance of the
98 Earth's climate system, especially in North China Plain (Wang et al., 2022a). As an important port
99 city in the North China Plain, Tianjin, which has a large population, has received a widespread
100 attention to address the atmospheric environmental issues. Previous studies have shown that BrC
101 in the atmosphere contributes significantly to the light absorption by aerosols (Deng et al., 2022).
102 PM_{2.5} loading in the Tianjin area is extremely high, with greater abundance of organic matter (OM)
103 (Dong et al., 2023a). In such an environment, BrC is likely to become an important light-absorbing
104 component of atmospheric aerosols. However, the studies on physico-chemical characteristics and
105 sources of BrC are very limited in the North China Plain, and to the best of our knowledge, the
106 long-term observations of the optical properties and molecular composition of BrC have not been
107 reported yet over the Tianjin region.

108 In this study, we measured the optical properties and molecular composition of WSBBrC and
109 water-insoluble but methanol-soluble BrC (WI-MSBrC) in fine aerosols (PM_{2.5}) collected from
110 Tianjin, North China over a one-year period using the combined UV-Vis absorption and EEM
111 fluorescence spectroscopy technique. We discussed the seasonal variations in optical properties
112 and chromophore composition of WSBBrC and WI-MSBrC in the PM_{2.5}. We also assessed the
113 possible sources of BrC including the potential photochemical processing of OA (aging) over the
114 Tianjin region, based on the relationships between the BrC and chemical tracers and stable carbon
115 ($\delta^{13}\text{C}$) and nitrogen ($\delta^{15}\text{N}$) isotope ratios of total carbon (TC) and nitrogen (TN) in the PM_{2.5}. Thus,
116 this study provides a comprehensive understanding of the optical characteristics, seasonality, and
117 sources of BrC in the Tianjin region, and warrant the need to develop the prevention and control
118 strategies for the BrC and/or its precursors emissions.

119 **2 Materials and Methods**

120 **2.1 Aerosol sampling**

121 Fine aerosol (PM_{2.5}) sampling was conducted in Tianjin, a coastal city located at the lower
122 reaches of the Haihe River and Bohai Sea and 150 km away from Beijing in the northern part of
123 China. The sampling took place on the rooftop of a six-storey building at Tianjin University (ND,
124 39.11°N, 117.18°E) in an urban area of Nankai District, Tianjin. A high-volume air sampler (Tisch
125 Environmental, TE-6070DX) at a flow rate of 1.0 m³ min⁻¹ and pre-combusted (6 hours at 450°C)
126 quartz fiber filters (Pallflex 2500QAT-UP) were used for continuously collecting the PM_{2.5}
127 samples for 3 days (~72 hours) each during 5 July 2018 to 4 July 2019 ($n = 121$). Filter blanks
128 were collected twice per season during the sample campaign, following the same sampling
129 procedure placing the filter in hood for 10 mins without turning on the sampler pump.

130 Prior to and after sampling, each filter was dehumidified in a desiccator for 48 hours and
131 determined the PM_{2.5} mass by gravimetric analysis, and then stored in a pre-combusted glass jar
132 with a Teflon-lined cap in the dark at -20°C until analysis.

133 2.2 Measurement of carbonaceous and ionic components

134 Details of the measurements of aerosol organic carbon (OC), element carbon (EC) and water-
135 soluble organic carbon (WSOC) were described by Wang et al. (Wang et al., 2019) and Dong et
136 al. (Dong et al., 2023a). Briefly, concentrations of the OC and EC were measured using an aliquot
137 of filter (1.5. cm²) and a thermal-optical carbon analyzer (Sunset Laboratory Inc, USA), following
138 the IMPROVE protocol of the protective visual environment. WSOC was measured using an
139 aliquot of filter (one disc of either 14 mm or 22 mm in diameter) extracted into organic-free Milli
140 Q water and total organic carbon (TOC) analyzer (Model OI, 1030W + 1088). Concentrations of
141 K⁺ and Cl⁻ were determined using an aliquot of filter (one disc of 22 mm in diameter) extracted
142 into ultrapure water (>18.2MΩ cm) and ion chromatography (ICS-5000 System, China, Dai An)
143 (Dong et al., 2023a). The analytical uncertainty in replicate analyses were within 2 % for OC and
144 5% for EC, WSOC and inorganic ions. Concentrations of all the components were corrected for
145 field blanks.

146 2.3 Measurement of optical properties of brown carbon (BrC)

147 2.3.1 Extraction and concentration of BrC

148 BrC was extracted into 30 ml ultrapure water using a sample filter disc of 22 mm in diameter
149 placed in a glass bottle with screw cap and sealed with Teflon tape under ultrasonication for 30
150 min. The extracts were filtered through a 0.45 μm polytetrafluoron (PTFE) syringe filter to remove
151 the water-insoluble particles and filter debris, and transferred into a clean glass bottle. The extracts
152 were used for the light absorption and fluorescence measurements of WSBrC. While the
153 concentration of WSBrC was considered as the concentration of WSOC.

154 After the extraction of WSBrC, the WI-MSBrC was extracted into 30 ml methanol using the
155 same filter sample left in the same glass bottle with screw cap sealed with Teflon tape under
156 ultrasonication for 30 min. The extracts were filtered using the same 0.45 μm PTFE syringe filter
157 to remove the insoluble particles and filter debris and transferred into another clean glass bottle.
158 The methanol extracts were used for the measurements of optical properties of WI-MSBrC. The
159 concentration of water-insoluble organic carbon (WIOC) was considered as the concentration of
160 WI-MSBrC, which calculated as equation (1), presuming that all the water-insoluble organic
161 contents are dissolved in methanol, although we do not preclude that some of organic species are
162 not soluble in MeOH (Shetty et al., 2019).

$$163 \quad WI - MSBrC = OC - WSOC \quad (1)$$

164 2.3.2 Light absorption of BrC

165 A three-dimensional fluorescence spectrometer (Aqualog, Horiba Scientific) was used to
166 record the excitation-emission matrices (EEM) spectra and ultraviolet-visible (UV-Vis)
167 absorption spectra of the solution samples in 1×1 cm quartz cuvettes. The instrument parameters
168 during sample analysis were as follows: The UV-Vis absorption spectra of extracts were recorded
169 in the wavelength range of 240–700 nm. The UV-visible absorption spectra of the solvents were
170 also recorded to subtract their contributions from the extract spectra. The EEM was recorded in
171 the wavelength range of 240–700 nm for excitation and the integration time was 0.1 s with a 1 nm

Deleted :

Deleted: WI-MSBrC = OC - WSOC,

Deleted: ¶

175 increment. An increment of 8 pixels (5.04 nm) is used as the emission wavelength interval. Prior
 176 to sample analysis, the pure solvents of water and methanol (MeOH) were used to obtain the
 177 reference signal.

178 Based on the light absorption spectra, the absorption data are converted to the absorption
 179 coefficient ($Abs: m^{-1}$) following equation (2) (Deng et al., 2022; Hecobian et al., 2010):

$$180 \quad Abs_{\lambda} = (A_{\lambda} - A_{700}) \times \frac{V_l}{V_a} \times \ln(10) \quad (2)$$

181 where A_{700} is the absorption at 700 nm, serving as a reference to account for baseline drift; V_l is
 182 the volume of water or MeOH used for extraction; V_a is the volume of sampled air; L is the optical
 183 path length (0.01 m). A factor of $\ln(10)$ is utilized to convert the log base 10 to a natural logarithm
 184 to obtain a base-e absorption coefficient. To compensate for any baseline shift that may occur
 185 during analysis, absorption at wavelengths below 700 nm is compared to that of 700 nm where no
 186 absorption occurs for ambient aerosol extracts. The average absorption coefficient between 360
 187 and 370 nm (Abs_{365}) is used to represent BrC absorption in order to avoid any interferences from
 188 non-organic compounds (e.g., nitrate) and to be consistent with the literature values (Huang et al.,
 189 2018).

190 Absorption Ångström exponent (AAE, Å) represents the spectral dependence of aerosol light
 191 absorption. The spectral dependence of light absorption by chromophores in solution can be
 192 described by the following equation (3):

$$193 \quad Abs_{\lambda} = C \times \lambda^{-AAE} \quad (3)$$

194 where C is a composition-dependent constant; λ is the wavelength (nm). The AAE of the filter
 195 extracts is calculated by a formula in the wavelength range of 300–500 nm. The selected range
 196 serves two purposes: (1) to prevent any interferences from non-organic compounds at lower
 197 wavelengths; (2) to ensure a sufficient signal-noise ratio for the investigating samples (Huang
 198 et al., 2018).

199 The mass absorption efficiency (MAE: $m^2 g^{-1}$) of the filter extract at wavelength of λ can be
 200 characterized as equation (4). The ratio of MAE₂₅₀ to MAE₃₆₅ is denoted as E_2/E_3 to characterize
 201 the relative size of molecular weight, which is inversely proportional to the molecular weight.
 202 E_2/E_3 is calculated with the method as equation (5).

$$203 \quad MAE_{\lambda} = Abs_{\lambda} / M \quad (4)$$

$$204 \quad \frac{E_2}{E_3} = \frac{MAE_{250}}{MAE_{365}} \quad (5)$$

205 where M ($\mu g m^{-3}$) is the concentration of WSOC for water extracts and that of WIOC for methanol
 206 extracts.

207 The imaginary part (k) of the refractive index ($m = n+ik$) is derived with the following
 208 equation (6) (Liu et al., 2013; Deng et al., 2022):

$$209 \quad k_{\lambda} = (MAE \times \rho \times \lambda) / 4\pi \quad (6)$$

210 where MAE is the mass-absorption cross section of WSBrC or WI-MSBrC ($m^2 g^{-1}$), ρ is the
 211 effective density, λ is the wavelength for the computed MAE including WSBrC and WI-MSBrC.
 212 For this study, an effective density of $1.5 g m^{-3}$ is assumed for WSBrC and WI-MSBrC in the
 213 derivation (Liu et al., 2013). MAE values are computed for 365 nm.

214 2.3.2 EEM of BrC and PARAFAC analysis

215 The raw EEMs were first calibrated for the correction of spectrometer factors, which reflect
 216 the spectrometer deviation and light source, and then for the inner filter correction, following the
 217 procedure described elsewhere (Chen et al., 2019; Gu and Kenny, 2009). Briefly, the inner filter

Deleted: this

Deleted: formula

Deleted: ¶

Deleted: $Abs_{\lambda} = (A_{\lambda} - A_{700}) \times V_l / V_a L \times \ln(10)$

Deleted: ¶

Deleted: $Abs_{\lambda} = C \times \lambda^{-AAE}$

Deleted: :

Deleted: ¶

Deleted: $MAE_{\lambda} = Abs_{\lambda} / M$

Deleted: $k_{\lambda} = (MAC \times \rho \times \lambda) / 4\pi$

Deleted: MAC

Deleted: MAC

Deleted: MAC

231 correction of the EEMs was done based on the UV-Vis light absorbance of the extracts, which was
 232 lower than 0.7 in the calibrated wavelength range and is appropriate (Gu and Kenny, 2009). The
 233 signal intensity of the EEMs was then normalized to the Raman unit (RU) of water (Lawaetz and
 234 Stedmon, 2009). The fluorescence volume (FV, RU-nm²/m³) of extracts present in the atmosphere
 235 was estimated based on the EEMs at the excitation wavelength ranging from 240 to 700 nm, and
 236 then normalized it (i.e., NFV (RU-nm²-[mg/L]⁻¹)) by dividing the FV with the concentration of
 237 WSOC and WIOC in the aerosol [mg m⁻³].

238 Various types of chromophores present in the PM_{2.5} samples were classified and identified
 239 based on the PARAFAC analysis of the EEMs using the SOLO (Eigenvector Inc.), the data
 240 analysis software. PARAFAC analysis was performed for each extraction fluid in each season.
 241 Ultimately, three EEM components were determined and assigned to different types of
 242 chromophores.

243 Additionally, fluorescence index (FI) was determined by calculating the ratio of emission
 244 intensities at 450 nm and 500 nm after excitation at 370 nm (McKnight et al., 2001). Contributions
 245 from local biological sources can be characterized by biological index (BIX), which was calculated
 246 using the ratio of emission intensities at 380 and 430 nm following 310 nm excitation (Gao yan
 247 and Zhang, 2018). Under the condition of Ex=255 nm, the humification index (HIX) was
 248 determined by dividing the area of fluorescence intensity between 435 and 480 nm by that of
 249 fluorescence intensity between 300 and 345 nm (Battin, 1998). The calculation formulas (7)– (9)
 250 are as follows:

$$251 \quad FI = \frac{F_{450}}{F_{500}}, \lambda_{Ex} = 370nm \quad (7)$$

$$252 \quad BIX = \frac{F_{380}}{F_{430}}, \lambda_{Ex} = 310nm \quad (8)$$

$$253 \quad HIX = \frac{\int_{300-345}^{435-480}}{\int_{300-345}}, \lambda_{Ex} = 255nm \quad (9)$$

254 In formula (6) - (8), λ_{Ex} refers to the excitation wavelength, F_i refers to the fluorescence
 255 intensity of emission wavelength at i in the emission spectrum, and $\int i-j$ refers to the integrated
 256 fluorescence emission intensity in the range of 435–480 nm to 300–345 nm.

257 2.3.3 Simple forcing efficiency by light absorption of BrC (SFE_{Abs})

258 It is possible to make a rough estimate of the radiative forcing caused by aerosols using a
 259 simple forcing efficiency (SFE, W/g), which reflects the energy added to the Earth's atmospheric
 260 system per unit mass of aerosols and can be estimated as described in the literature (Bond and
 261 Bergstrom, 2006; Deng et al., 2022), using the following equation (10):

$$262 \quad \frac{dSFE}{d\lambda} = -\frac{1}{4} \frac{dS(\lambda)}{d\lambda} \tau_{atm}^2(\lambda)(1 - F_c) [2(1 - a_s)^2 \beta(\lambda) \times MSE(\lambda) - 4a_s \times MAE(\lambda)] \quad (10)$$

263 where $dS/d\lambda$ is the solar irradiance, τ_{atm} is the atmospheric transmission (0.79), F_c is the cloud
 264 fraction (approximately 0.6), a is the surface albedo (average 0.19), β is the backscatter fraction,
 265 and MSE and MAE are the mass scattering and absorption efficiency, respectively (Deng et al.,
 266 2022).

267 Since BrC causes the radiative effect mainly by light absorption, rather than the scattering
 268 that has stronger dependency on the particle size, we limited to estimate the radiative effect caused
 269 by only the absorption of the BrC in this study. Therefore, the equation (10) can be simplified to:

$$270 \quad SFE_{Abs} = \int \frac{dS(\lambda)}{d\lambda} \tau_{atm}^2 (1 - F_c) a_s MAE(\lambda) d\lambda \quad (11)$$

Deleted: ¶

Deleted: ¶

$$\frac{dSFE}{d\lambda} = -\frac{1}{4} \frac{dS(\lambda)}{d\lambda} \tau_{atm}^2(\lambda)(1 - F_c) [2(1 - a_s)^2 \beta(\lambda)$$

Deleted: only

Deleted: direct radiative forcing due to aerosol

Deleted: can be ignored when estimating

3 Results and discussion

3.1 Characteristics of ultraviolet light absorption of WSBrc and WI-MSBrc

3.1.1 Absorption coefficient (Abs)

Annual and seasonal averages of various optical properties of WSBrc and WI-MSBrc in PM_{2.5} measured in this study are summarized in Table 1. Their ranges and median values are provided in supplement Table S1. Temporal variations in absorption coefficient of WSBrc at 365 nm (Abs_{365(WSBrc)}) and that of WI-MSBrc (Abs_{365(WI-MSBrc)}) together with the concentrations of WSOC and WIOC are depicted in Fig. 1. Because the light absorption at the wavelength of 365 nm would not be interfered by inorganic substances (Hecobian et al., 2010), the Abs at 365 nm was selected for the analysis in this study. Abs_{365(WSBrc)} ranged from 0.49 Mm⁻¹ to 36.7 Mm⁻¹ with an average of 4.74 Mm⁻¹ during the campaign. While the Abs_{365(WI-MSBrc)} ranged from 0.32-25.0 Mm⁻¹ (avg. 3.87 Mm⁻¹) during the campaign. Temporal trends of Abs_{365(WSBrc)} were found to be similar with those of Abs_{365(WI-MSBrc)}, with the lowest levels in summer followed by a gradual increase toward autumn and peak in winter and then a gradual decrease toward spring during the campaign (Fig. 1). Furthermore, those trends were highly comparable to those of the concentrations of both WSOC and WIOC in PM_{2.5} (Fig. 1). The correlations between Abs_{365(WSBrc)} and WSOC and Abs_{365(WI-MSBrc)} and WIOC were found to be strong (R = 0.93 and 0.96, respectively) during the campaign. These results indicate that both WSBrc and WI-MSBrc might have been derived from the same or similar sources including the secondary processes, and their light absorbance should have been significantly dependent on their abundances that varied from season to season (Fig. 1; Table 1).

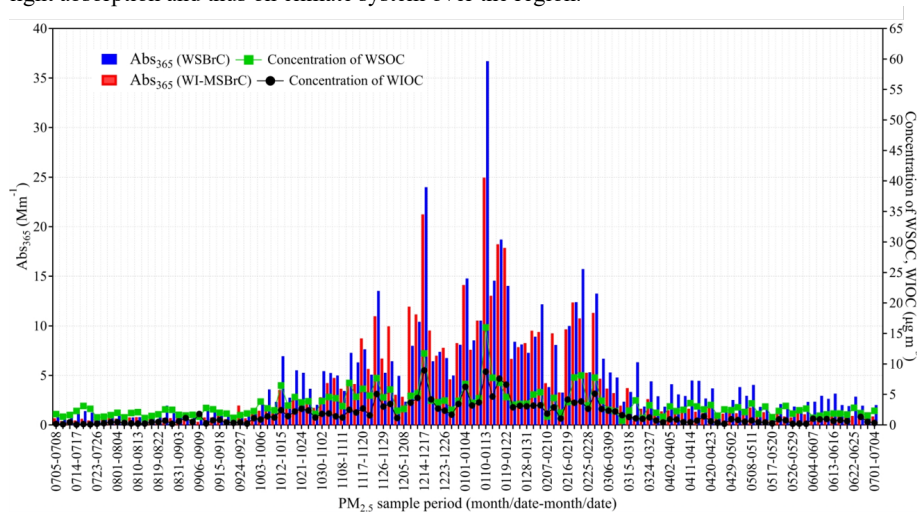
Averages of both Abs_{365(WSBrc)} and Abs_{365(WI-MSBrc)} were higher in winter followed by autumn and spring and the lowest in summer (Table 1). The high Abs₃₆₅ of BrC in winter might have been mainly driven by the existence of large amounts of organic aerosols, whereas the lowest Abs₃₆₅ in summer might be due to enhanced decomposition of BrC constituents by photobleaching under high solar radiation and oxidants loading in the atmosphere, which is unlikely in the wintertime. The seasonal variations of both Abs_{365(WSBrc)} and Abs_{365(WI-MSBrc)} in Tianjin were similar to those of the Abs₃₆₅ of WSBrc reported in the southeastern United States, but their values (Table 1) were much higher than that (0.3–3.0 Mm⁻¹ in 2007) in the southeastern United States (Hecobian et al., 2010) as well as that in Atlanta and Los Angeles (0.88 ± 0.71 and 0.61 ± 0.38 Mm⁻¹, respectively) in summer 2010 (Zhang et al., 2011). Biomass burning was considered to be the dominant source of BrC at the southeastern United States in colder period, whereas both primary emissions from fossil fuel combustion and secondary formation were significant in summertime (Hecobian et al., 2010). While the SOA formed from fresh anthropogenic and biogenic VOCs were considered to be major at Atlanta and Los Angeles, respectively (Zhang et al., 2011).

It has been reported that the solid fuels (i.e., biomass or coal) combustion is dominant and the Abs₃₇₀ of BrC is reported to be high (21.8 Mm⁻¹) in North China cities (Zhang et al., 2021). It has also been reported that the Abs₃₇₀ of BrC produced by residential wood burning is much higher, reaching up to 37.1 ± 74.6 Mm⁻¹ in Athens in winter (Liakakou et al., 2020). The maximum Abs_{365(WSBrc)} and Abs_{365(WI-MSBrc)} in Tianjin aerosols were 36.7 and 25.0 Mm⁻¹, respectively, which are comparable to those of wood combustion samples. However, their ranges found to be large during the campaign (Fig. 1; Table S1), suggesting that in addition to biomass burning, the other emission sources and meteorological conditions in different seasons should have been played

$$\text{Deleted: } SFE = \int \frac{dS(\lambda)}{d\lambda} \tau_{am}^2 (1 - F_c) a_s MAE(\lambda) d\lambda$$

Deleted: ave

323 an important role in controlling the WSB_{rC} and WI-MSBrC loadings and their optical
 324 characteristics in the Tianjin atmosphere. Furthermore, the Abs₃₆₅(WSBrC) observed in this study
 325 (Table 1) is slightly lower compared to that reported in Tianjin during winter 2016 (14.1 ± 8.5
 326 Mm^{-1}) and summer 2017 ($2.1 \pm 1.0 \text{Mm}^{-1}$) (Deng et al., 2022) as well as that reported in Beijing
 327 and Xi'an, which are considered to be highly polluted cities in northern China (Huang et al.,
 328 2020; Li et al., 2020b). However, the Abs₃₆₅(WSBrC) and Abs₃₆₅(WI-MSBrC) found in winter in this study
 329 were higher than that reported at different locations in southern China; Nanjing (Abs₃₆₅(WSBrC) =
 330 4.84Mm^{-1} , Abs₃₆₅(MSBrC) = 7.75Mm^{-1}) (Xie et al., 2020), Guangzhou (Abs₃₆₅(WSBrC) = 8.8Mm^{-1})
 331 (Li et al., 2018), and Lhasa (Abs₃₆₅(WSBrC) = 1.04Mm^{-1} , Abs₃₆₅(MSBrC) = 1.47Mm^{-1}) (Zhu et al.,
 332 2018), where the fossil fuel combustion is considered as the dominant source. Such higher Abs₃₆₅,
 333 particularly in winter, indicates that BrC in PM_{2.5} in Tianjin might have been derived from mixed
 334 sources such as biomass burning and fossil fuel (coal) combustion and has a significant effect on
 335 light absorption and thus on climate system over the region.

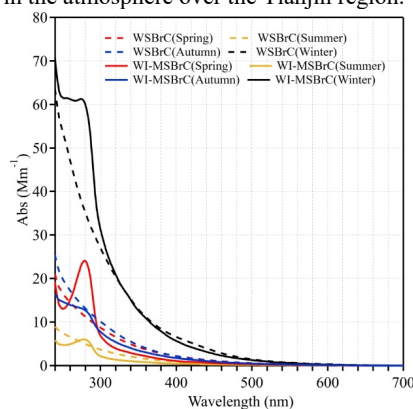


336
 337 **Figure 1.** Temporal variations of the light absorption coefficient of water-soluble brown carbon
 338 (BrC) at 365 nm (Abs₃₆₅(WSBrC)) and water-insoluble but methanol-soluble BrC (Abs₃₆₅(WI-MSBrC))
 339 and the mass concentrations of WSOC and WIOC in PM_{2.5} in Tianjin, North China during 2018
 340 and 2019. WSOC and WIOC mass concentrations data was obtained from (Dong et al., 2023b).

341 Figure 2 shows the seasonal average absorption spectra of WSB_{rC} and WI-MSBrC at
 342 wavelengths of 240–700 nm, which shows a common feature that the absorption of shorter
 343 wavelengths increases sharply and significantly. Such feature is different from the absorption
 344 characteristics of BC, whose AAE is close to 1 and weakly dependent on the wavelength. Another
 345 evident feature of BrC absorption spectra shown in Figure 2 is that the Abs of WI-MSBrC was
 346 always greater than that of WSB_{rC} across the shorter wavelengths in winter and in the range of
 347 260–300 nm in other seasons, which is consistent with the pattern reported in the literature (Huang
 348 et al., 2020; Li et al., 2020b). In addition, the Abs of WI-MSBrC peaked at 280 nm, but not that of
 349 WSB_{rC} (Fig. 2). Such patterns can be attributed to the difference in types and amounts of

350 chromophores soluble in water and methanol (e.g., PAHs are soluble in methanol, but not in water).
351 It is noteworthy that, $\pi-\pi^*$ electron transitions in the double bonds of aromatic compounds are the
352 primary cause of light absorption in the wavelength range of 250–300 nm. It has been reported in
353 another study that nitroaromatics have contributed 60% to the total absorbance in the 300-400 nm
354 range (Hems et al., 2021). The electron transitions in phenolic arenes, aniline derivatives, polyenes
355 and polycyclic aromatic hydrocarbons with two or more rings are responsible for the absorbance
356 in the bands between 270 and 280 nm (Baduel et al., 2009). Therefore, the differences observed in
357 the Abs of WSB_{BrC} and WI-MSB_{BrC} imply that the aromatic and/or unsaturated aliphatic organic
358 compounds are abundant in PM_{2.5} in Tianjin, which are more soluble in MeOH than in water.

359 High correlations ($R = 0.73-0.97$) were found between Abs₃₆₅ of both WSB_{BrC} and WI-
360 MSB_{BrC} and WSOC and WIOC in each season, except in summer ($R = 0.20-0.62$) (Figure S1). As
361 noted earlier, such linearity of Abs₃₆₅ with WSOC and WIOC indicate that WSB_{BrC} and WI-
362 MSB_{BrC} might have been derived from similar sources including the secondary processes over the
363 Tianjin region, except in summer, because the light absorption efficiency of organic compounds
364 of different origin are different and significantly depend on their secondary processes in the
365 atmosphere (Zhong and Jang, 2011). In fact, the Abs depends on the amount of BrC availability,
366 but not of total OC content. In summer, the BrC loading might be less due to either photobleaching
367 under the enhanced aging and/or less availability of N and/or S species to produce N- and S-
368 containing organics (BrC) in the atmosphere over the Tianjin region.



369

370 **Figure 2.** Seasonal averages of absorption spectra in the wavelength range of 240–700 nm of
371 WSB_{BrC} and WI-MSB_{BrC} in PM_{2.5} from Tianjin, North China.

372 The moderate to high positive correlations ($R = 0.51-0.92$) found between both Abs₃₆₅(WSB_{BrC})
373 and Abs₃₆₅(WI-MSB_{BrC}) and K⁺ and Cl⁻ in all seasons, except between Abs₃₆₅ WSB_{BrC} and Cl⁻ in summer
374 ($R = 0.29$) (Fig. S2), suggest that biomass burning and coal combustion were major sources (Dong
375 et al., 2023a) of BrC in the Tianjin region. The poor correlation between Abs₃₆₅ and K⁺ was driven
376 by two outliers obtained in K⁺ data that might have occurred due to unknown biomass burning
377 events at local scale. In addition, the correlation between Abs₃₆₅(WSB_{BrC}) and K⁺ was relatively
378 stronger than that between the Abs₃₆₅(WI-MSB_{BrC}) and K⁺, except in summer (Fig. S2), which support
379 that the chromophores, like nitrophenols, derived from biomass burning are potentially more
380 water-soluble (Li et al., 2020b). While the correlation between Abs₃₆₅(WI-MSB_{BrC}) and Cl⁻ was

381 relatively stronger than that between $Abs_{365}(WSBrC)$ and Cl^- in spring and summer and comparable
382 in autumn, which suggest that the chromophores derived from fossil fuel (e.g., coal) combustion
383 are slightly more soluble in MeOH compared to that in water, and were abundant in the spring and
384 summer time in Tianjin.
385

Table 1. Mass concentrations of WSOC, WIOC, and absorbance efficiency of WSBrc and WI-MSBrC (Avg. \pm SD) in PM_{2.5} from Tianjin, North China.

	Annual	Summer	Autumn	Winter	Spring
Concentrations					
WSOC ($\mu\text{g m}^{-3}$)	3.25 \pm 2.18	1.88 \pm 0.53	3.45 \pm 1.71	5.06 \pm 2.99	2.48 \pm 0.82
WIOC ($\mu\text{g m}^{-3}$)	1.68 \pm 1.77	0.43 \pm 0.32	1.55 \pm 1.04	3.74 \pm 2.09	0.88 \pm 0.63
Optical parameters					
Abs ₃₆₅ (Mm ⁻¹)	4.74 \pm 5.10	1.47 \pm 0.77	3.71 \pm 2.83	10.4 \pm 6.76	3.45 \pm 2.29
MAE ₃₆₅ (m ² g ⁻¹)	1.28 \pm 0.66	0.80 \pm 0.44	0.96 \pm 0.33	2.04 \pm 0.46	1.31 \pm 0.55
AAE (300–500 nm)	5.66 \pm 0.82	5.17 \pm 0.83	6.21 \pm 0.65	5.88 \pm 0.58	5.42 \pm 0.74
E ₂ /E ₃	5.64 \pm 1.21	5.64 \pm 1.21	5.78 \pm 0.83	5.19 \pm 0.44	4.83 \pm 0.64
FI	1.38 \pm 0.09	1.31 \pm 0.07	1.47 \pm 0.07	1.37 \pm 0.02	1.37 \pm 0.09
BIX	1.05 \pm 0.13	0.91 \pm 0.06	1.06 \pm 0.08	1.20 \pm 0.08	1.01 \pm 0.11
HIX	2.87 \pm 0.53	3.12 \pm 0.44	3.11 \pm 0.51	2.47 \pm 0.43	2.76 \pm 0.47
k ₃₆₅	0.056 \pm 0.029	0.035 \pm 0.020	0.042 \pm 0.015	0.089 \pm 0.021	0.057 \pm 0.024
SFE _{Abs300-400} (W g ⁻¹)	1.95 \pm 1.02	1.21 \pm 0.67	1.99 \pm 0.84	3.12 \pm 0.71	1.46 \pm 0.52
SFE _{Abs300-700} (W g ⁻¹)	4.97 \pm 2.71	3.68 \pm 2.58	5.12 \pm 2.17	7.60 \pm 2.17	3.39 \pm 1.42
Abs ₃₆₅ (Mm ⁻¹)	3.87 \pm 4.69	0.74 \pm 0.25	2.83 \pm 2.51	10.0 \pm 5.13	1.99 \pm 1.95
MAE ₃₆₅ (m ² g ⁻¹)	2.36 \pm 1.26	2.50 \pm 1.78	1.86 \pm 1.02	2.69 \pm 0.36	2.41 \pm 1.28
AAE (300–500 nm)	6.06 \pm 1.23	5.49 \pm 1.26	6.11 \pm 1.86	6.30 \pm 0.27	6.27 \pm 0.90
E ₂ /E ₃	6.60 \pm 2.04	6.79 \pm 1.32	5.77 \pm 1.35	6.20 \pm 0.44	7.60 \pm 3.25
FI	1.60 \pm 0.13	1.58 \pm 0.12	1.57 \pm 0.06	1.73 \pm 0.11	1.51 \pm 0.11
BIX	1.26 \pm 0.21	1.32 \pm 0.18	1.05 \pm 0.14	1.43 \pm 0.09	1.23 \pm 0.18
HIX	0.81 \pm 0.60	0.25 \pm 0.08	1.23 \pm 0.61	1.33 \pm 0.30	0.42 \pm 0.28
k ₃₆₅	0.104 \pm 0.057	0.109 \pm 0.079	0.081 \pm 0.045	0.117 \pm 0.016	0.105 \pm 0.057
SFE _{Abs300-400} (W g ⁻¹)	2.98 \pm 1.70	1.21 \pm 0.67	2.98 \pm 1.52	4.13 \pm 0.57	3.61 \pm 1.91
SFE _{Abs300-700} (W g ⁻¹)	7.58 \pm 5.75	3.68 \pm 2.58	8.69 \pm 9.23	9.36 \pm 4.51	8.70 \pm 5.03

Deleted: Ave

Formatted: Subscript

Formatted: Subscript

Formatted: Subscript

388 3.1.2 Absorption Ångström exponent (AAE)

389 The magnitude of the AAE can reflect the sources and atmospheric chemical processes of
390 BrC (Lack et al., 2013), because the AAE of the BrC emitted from fossil fuel combustion found
391 to be ~1 and that from biomass burning range from 1 to 3 and that derived by secondary
392 formation/transformations vary from 3-7 (Yan et al., 2018). It has also been reported that the AAE
393 of light-absorbing organic species (i.e., BrC) is much larger than that of soot (BC). The AAE was
394 found to be between 2 and 4 for the particles containing both soot and BrC. Furthermore, AAE
395 value of particulate matter is closely related to its chemical composition, mixing state, particle size
396 and other factors. For example, Sun et al. (2007) reported that the average AAE of coal briquettes
397 is 2.55 ± 0.44 whereas that of the coal chunks is 1.30 ± 0.32 (Sun et al., 2017). However, it is
398 important to note that unlike the direct measurement of AAE of the particulate matter, the light
399 absorption characteristics of organic components extracted into solvent are not affected by particle
400 size and mixing state of aerosols, but depend on their composition. The AAE of humic-like
401 substances (HULIS) isolated from biomass burning aerosols by water extraction followed by the
402 separation with exchange column was reported to be 6-7 (Hoffer et al., 2006).

403 The AAE of WSBrc in PM_{2.5} from Tianjin ranged from 3.85 to 7.99 with an average of 5.66
404 during the campaign. The seasonal averages were highly comparable with each other, except a
405 little higher level in autumn (Table 1). The average AAE of WSBrc in Tianjin (Table 1) is
406 comparable to that (5.1 ± 2.0) reported from New Delhi, India and Beijing (5.3 ± 0.4 in winter and
407 5.8 ± 0.5 in summer) and the outflow region (6.4 ± 0.6) of northern China (Lesworth et al., 2010).
408 The AAE of WSBrc in Tianjin was also similar to that (range, 6–8) reported in the particulate
409 matter at the southeastern United States (Hecobian et al., 2010) and downtown Atlanta (Liu et al.,
410 2013), where both biogenic and fossil fuel combustion emissions and secondary processes are
411 considered as significant sources. Such higher levels and comparisons of the AAE of WSBrc
412 imply that the OA in Tianjin should have been derived from mixed sources and substantially polar,
413 because the AAE of BrC is increased with its increasing polarity (Chen et al., 2016a).

414 However, the AAE of WI-MSBrC in Tianjin ranged from 2.08–12.9 (avg. 6.06) and was
415 comparable with that of WSBrc. Furthermore, the averages of AAE of WI-MSBrC in each season
416 were comparable with the other, except a relatively lower level in summer, and also with those of
417 the AAE of WSBrc (Table 1). Generally, the water insoluble portion is expected to have a stronger
418 absorption and weaker wavelength dependence (Saleh, 2020). It has also been reported that the
419 AAE values of the water extract are greater than those of the acetone and methanol extracts (Shetty
420 et al., 2019), and interpreted that the extraction efficiency of polycyclic aromatic hydrocarbons
421 from methanol or other organic solvents is higher than that from water, leading to a higher
422 absorption at longer wavelengths in the methanol extract and therefore a lower AAE value.
423 However, it has also been found that the value of AAE₃₀₀₋₆₀₀ of water extract of biomass burning
424 samples is lower than that extracted into acetonitrile (Lin et al., 2017), indicating that the origin of
425 the BrC is also play an important role. Such comparability between the AAE of WSBrc and WI-
426 MSBrC is consistent with the pattern reported in urban Beijing during winter and Xi'an, China (Li
427 et al., 2020b), where the emissions from fossil fuel combustion are dominant. These results and
428 their comparisons again support that the BrC might have significantly derived from mixed sources
429 (biomass burning and fossil fuel combustion).

Deleted:

Deleted: ave

Deleted: (Chen et al., 2016b)

Deleted: In fact, the AAE of the solvent (e.g., acetonitrile) extracted portion of the BrC derived from biomass burning is also large (Lin et al., 2017).

436 3.1.3 Mass absorption efficiency (MAE) and imaginary refractive index (k)

437 MAE provides the light absorbing ability of BrC. The MAE₃₆₅ of WSB_{rC} (MAE_{365(WSB_{rC})})
438 ranged from 0.38 m² g⁻¹ to 3.41 (avg. 1.28 m² g⁻¹) and lower by 2 times than that (range, 0.18-7.05
439 m² g⁻¹; avg. 2.36 m² g⁻¹) of WI-MSB_{rC} (MAE_{365(WI-MSB_{rC})}) during the campaign in Tianjin.
440 Although the seasonal averages of both MAE_{365(WSB_{rC})} and MAE_{365(WI-MSB_{rC})} were higher in winter
441 (1.28 and 2.36 m² g⁻¹, respectively), the former showed the second most value in spring followed
442 by autumn and the lowest value in summer, whereas the latter showed second most value in
443 summer followed by spring and the lowest value in autumn (Table 1). Furthermore, the average
444 MAE_{365(WSB_{rC})} in winter was 2.5 times higher than that in summer, which is similar to that (1.8
445 times) reported earlier in Tianjin (Deng et al., 2022), whereas the difference between the averages
446 of MAE_{365(WI-MSB_{rC})} in winter to autumn is 1.4 times only. The seasonal variations of MAE_{365(WSB_{rC})}
447 and MAE_{365(WI-MSB_{rC})} found in this study are similar to those reported in Xi'an (Li et al., 2020b).

448 The imaginary refractive index (k) is another important parameter that represent the light
449 absorbing ability of carbon and applied in climate model to assess the direct radiative forcing of
450 aerosols. The k of WSB_{rC} ($k_{365(WSB_{rC})}$) and WI-MSB_{rC} ($k_{365(WI-MSB_{rC})}$) in Tianjin ranged from
451 0.017 to 0.149, and 0.008-0.307, respectively, in Tianjin. Interestingly, the average $k_{365(WI-MSB_{rC})}$
452 was 1.9 times to that of $k_{365(WSB_{rC})}$ during the campaign (Table 1) and their seasonal patterns were
453 also exactly similar to those of the MAE_{365(WSB_{rC})} and MAE_{365(WI-MSB_{rC})} (Table 1).

454 Both these MAE₃₆₅ and k_{365} results indicate that most of light-absorbing chromophores are
455 insoluble in water but soluble in MeOH, and their abundances are significantly varied from season
456 to season. Such large seasonal differences indicate that the BrC sources and formation and/or
457 transformation including the degradation (photobleaching) processes might be different in each
458 season. The higher levels of MAE₃₆₅ and k_{365} in winter suggest that the contributions of OA from
459 coal combustion and biomass burning emissions were significantly higher than that in other
460 seasons due to increased residential heating activities. The lower MAE_{365(WSB_{rC})} and $k_{365(WSB_{rC})}$ and
461 the second most values of MAE_{365(WI-MSB_{rC})} and $k_{365(WI-MSB_{rC})}$ in summer imply that the
462 contributions of OA from fossil fuel combustion emissions might be dominant and the subsequent
463 photobleaching of WSB_{rC} might be significant under high solar radiation in the summertime.

464 The ratio of MAE₂₅₀ to MAE₃₆₅, which is inversely correlate with the molecular size and
465 aromaticity (Chen et al., 2016c), of WSB_{rC} ($E_2/E_3(WSB_{rC})$) and WI-MSB_{rC} ($E_2/E_3(WI-MSB_{rC})$) in
466 Tianjin ranged from 3.30 to 6.25 with an average of 4.83 and 4.50-24.1 (avg. 7.61), respectively,
467 during the campaign. Interestingly, the averages of $E_2/E_3(WSB_{rC})$ were comparable in summer and
468 autumn and higher than that in winter and spring (Table 1). Whereas the average $E_2/E_3(WI-MSB_{rC})$
469 was higher in spring followed by summer and winter and the lowest in autumn, and higher than
470 the $E_2/E_3(WSB_{rC})$ in each season, except in autumn. Both $E_2/E_3(WSB_{rC})$ and $E_2/E_3(WI-MSB_{rC})$ in each
471 season were comparable or relatively higher than the E_2/E_3 of HULIS (4.7 ± 0.27 for herbaceous
472 plants, 3.6 ± 0.18 for shrubs, 4.2 ± 0.77 for evergreen trees, 4.0 ± 0.82 for deciduous trees, $5.8 \pm$
473 0.5 for rice straw, 4.5 ± 0.2 for corn straw and 4.4 ± 0.3 for pine branches) emitted from biomass
474 burning (Tang et al., 2020) and lower than that (14.7 ± 0.7) of HULIS emitted from coal
475 combustion (Fan et al., 2016). Thus, the $E_2/E_3(WSB_{rC})$ and $E_2/E_3(WI-MSB_{rC})$ and their comparisons
476 with source signatures indicate that both WSB_{rC} and WI-MSB_{rC} in PM_{2.5} over the Tianjin region
477 should have been mainly derived from biomass burning followed by coal combustion and consist
478 of high aromaticity and large in molecular size.

Deleted: ave

Deleted: ave

Deleted: (ave.

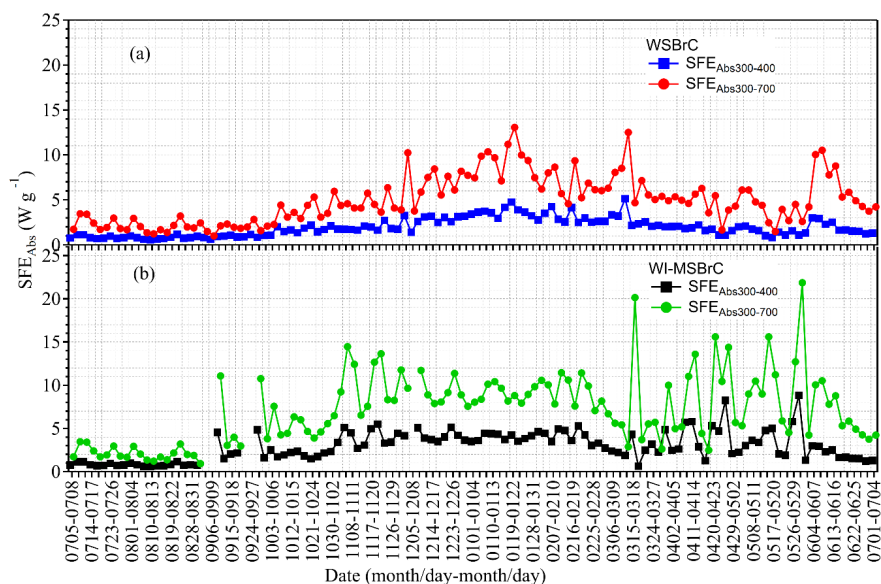
Deleted: ave

484 Radiative forcing efficiency of WSBrc and WI-MSBrc were calculated by integrating the
 485 wavelength dependent SFE_{Abs} from 300 nm to 700 nm ($SFE_{Abs300-700(WSBrc)}$ and $SFE_{Abs300-700(WI-MSBrc)}$, respectively) in this study. The $SFE_{Abs300-400}$ was also integrated to estimate the radiative
 486 forcing efficiency of WSBrc ($SFE_{Abs300-400(WSBrc)}$) and WI-MSBrc ($SFE_{Abs300-400(WI-MSBrc)}$),
 487 because the BrC strongly absorbs light in the UV-Vis range. The temporal variations of SFE_{Abs} of
 488 WSBrc and WI-MSBrc in both the wavelength ranges are shown in Fig. 3. $SFE_{Abs300-700(WSBrc)}$
 489 and $SFE_{Abs300-400(WSBrc)}$ ranged from 0.98 Wg^{-1} to 13.1 Wg^{-1} with an average of 4.97 Wg^{-1} and
 490 0.60-5.13 Wg^{-1} (avg. 1.95 Wg^{-1}), respectively. Whereas the $SFE_{Abs300-700(WI-MSBrc)}$ and $SFE_{Abs300-400(WI-MSBrc)}$
 491 were 0.92-51.3 Wg^{-1} (7.58 Wg^{-1}) and 0.64-8.84 Wg^{-1} (2.98 Wg^{-1}), respectively, and
 492 were higher by 1.5 times than that of the $SFE_{Abs300-700(WSBrc)}$ and $SFE_{Abs300-400(WSBrc)}$ (Table 1).
 493 Further both integrated average $SFE_{Abs300-700(WSBrc)}$ and $SFE_{Abs300-700(WI-MSBrc)}$ were higher by 2.5
 494 times to that of the $SFE_{Abs300-400(WSBrc)}$ and $SFE_{Abs300-400(WI-MSBrc)}$ (Table 1). Temporal variations
 495 of both the $SFE_{Abs300-400(WSBrc)}$ and $SFE_{Abs300-700(WSBrc)}$ were found to be quite similar with a clear
 496 seasonal pattern with the lowest levels in summer followed by a gradual increase toward autumn
 497 to peak in winter and then a gradual decrease toward spring to the lowest levels in summer, except
 498 a sharp rise in early summer 2019 (Fig. 3). Whereas the $SFE_{Abs300-400(WI-MSBrc)}$ and $SFE_{Abs300-700(WI-MSBrc)}$
 499 showed exactly the similar temporal pattern with each other, but different from that of the
 500 $SFE_{Abs300-400(WSBrc)}$ and $SFE_{Abs300-700(WSBrc)}$ (Fig.3). The levels of $SFE_{Abs300-400(WI-MSBrc)}$ and
 501 $SFE_{Abs300-700(WI-MSBrc)}$ found to be relatively stable throughout each season, except in spring, with
 502 higher level in spring followed by winter and lower levels in summer (Fig. 3). In consistent with
 503 these seasonal patterns, the seasonal variations of $k_{365(WSBrc)}$ and $k_{365(WI-MSBrc)}$, a vital parameter
 504 that reflect the light absorbing ability and used in the estimation of radiative forcing by climatic
 505 model (Shamjad et al., 2016), were also showed the similar pattern (Fig. S3).

507 The SFE_{Abs} of both WSBrc and WI-MSBrc in both the spectral ranges were higher in winter
 508 (Table 1). However, $SFE_{Abs300-400(WSBrc)}$ and $SFE_{Abs300-700(WSBrc)}$ showed the second higher values
 509 in autumn and the lowest and comparable values in summer and spring (Table 1). Whereas
 510 $SFE_{Abs300-400(WI-MSBrc)}$ and $SFE_{Abs300-700(WI-MSBrc)}$ showed the second higher and comparable values
 511 in spring and autumn and the lowest values in summer (Table 1). It is noteworthy that the
 512 $SFE_{Abs300-400(WSBrc)}$, $SFE_{Abs300-700(WSBrc)}$, $SFE_{Abs300-400(WI-MSBrc)}$ and $SFE_{Abs300-700(WI-MSBrc)}$ were
 513 higher by 61%, 52%, 71% and 61%, respectively, in winter than those in summer, indicating that
 514 BrC abundance and strong light absorption capacity of BrC in winter led to a significant increase
 515 in direct radiative forcing by the BrC. Furthermore, $SFE_{Abs300-400}$ accounted for 40% of $SFE_{Abs300-700}$
 516 in both the fractions of BrC during the whole campaign period and their seasonal averages
 517 varied between 33-44%, which are similar to that reported in Tianjin by Deng et al. (2022),
 518 indicating the light absorption by BrC in UV-Vis range play a significant role in the total BrC
 519 radiative forcing.

520 Furthermore, it is important to note that it has been reported that direct radiative effect of
 521 WSBrc is 12.5%% and 13.5% relative to black carbon (BC) radiative forcing in the 280-4000 nm
 522 range in summer and winter, respectively, in Tianjin (Deng et al., 2022). In fact, as noted above,
 523 the annual average $SFE_{Abs300-700(WI-MSBrc)}$ is higher by 1.5 times to that of $SFE_{Abs300-700(WSBrc)}$
 524 (Table 1) in Tianjin. Therefore, the direct radiative effect of total ($\Sigma WSBrc+WI-MSBrc$) BrC
 525 relative to BC would become ~32.5% in Tianjin, revealing that the BrC play a greater role in light
 526 absorbing aerosols in the shorter wavelength region in comparison to the entire spectrum.

Deleted: ave



528

529 **Figure 3.** Temporal variations in SFE_{Abs} of WSBrc and WI-MSBrc from 300–400nm and 300–
 530 700nm in $PM_{2.5}$ from Tianjin.

531 3.3 Fluorescence characteristics of WSBrc and WI-MSBrc

532 3.3.1 Fluorescence indices

533 Annual and seasonal averages of the fluorescence indices: FI, BIX and HIX, of WSBrc
 534 (FI_{WSBrc} , BIX_{WSBrc} and HIX_{WSBrc} , respectively) and WI-MSBrc ($FI_{WI-MSBrc}$, $BIX_{WI-MSBrc}$ and
 535 $HIX_{WI-MSBrc}$, respectively) in $PM_{2.5}$ at Tianjin are presented in Table 1. Their ranges and median
 536 values are provided in Table S1, and temporal variations are depicted in Fig. 3. Fluorescence
 537 indices are developed as indicators for the type and source of the fluorescent organic matter (OM)
 538 in aquatic and soil systems and has been successfully applied to assess the sources and aging
 539 processes of OA in the atmosphere in recent times (Dong et al., 2023b; Lee et al., 2013; Wu et al.,
 540 2021b). FI and BIX provide the insights in exploring the source and aging of OA and received
 541 much attention in recent times (Xie et al., 2020; Gao yan and Zhang, 2018; Qin et al., 2018; Deng
 542 et al., 2022). They have been considered as indicators to assess the relative contributions of
 543 terrestrial, biological and microbially derived OM to OA. The FI values of OM lower than 1.4
 544 indicate its terrestrial origin and the values of 1.9 or higher indicate the microbial origin, and shows
 545 an inverse relationship with aromaticity of the OM (Gao yan and Zhang, 2018; Birdwell and Engel,
 546 2010). The BIX values of 0.8 and 1.0 correspond to the freshly derived OM of biological or
 547 microbial origin and those of ~0.6 imply the little contribution of the biological OM (Birdwell and
 548 Engel, 2010; Dong et al., 2023b). HIX reflect the degree of humification of OA, and has been
 549 considered as a proxy for aromaticity of OM and the HIX value is increased with the increasing

550 aromaticity and polycondensation degree (Deng et al., 2022;McKnight et al., 2001;Birdwell and
551 Engel, 2010). The HIX values of >5 reflect the fresh OM derived from biomass and animal manure
552 (Birdwell and Engel, 2010).

553 FI_{WSBrC} and $FI_{WI-MSBrC}$ were ranged from 1.13 to 1.63 with an average of 1.38 and 1.29-2.24
554 (avg. 1.60), respectively, during the campaign in Tianjin. While BIX_{WSBrC} and $BIX_{WI-MSBrC}$ were
555 0.79-1.39 (1.05) and 0.83-1.76 (1.26), respectively, during the campaign. Both FI and BIX of
556 $WSBrC$ and $WI-MSBrC$ followed a temporal pattern, but the temporal pattern of FI_{WSBrC} was
557 exactly opposite to that of the $FI_{WI-MSBrC}$ (Fig. 4a). The FI_{WSBrC} values were slightly decreased
558 from summer to autumn followed by a gradual increase to mid-winter and then a gradual decrease
559 to summer through spring (Fig. 4a). While the temporal variations of BIX_{WSBrC} showed a gradual
560 decrease from summer to autumn followed by a gradual increase to winter and remained relatively
561 stable during the wintertime followed by a gradual decrease to to summer through spring (Fig. 4b).
562 The temporal variations of $BIX_{WI-MSBrC}$ were also found to be opposite to those of the BIX_{WSBrC} ,
563 except in winter, in which the $BIX_{WI-MSBrC}$ values were higher compared to those in other seasons
564 (Fig. 4b). Interestingly, the temporal patterns of HIX_{WSBrC} and $HIX_{WI-MSBrC}$ were found to be
565 similar with relatively stable in summer followed by a sharp increase in early autumn and then a
566 gradual decrease to summer through winter and spring (Fig. 4c). Further the HIX_{WSBrC} was always
567 significantly higher than the $HIX_{WI-MSBrC}$. Such temporal differences in all the three fluorescence
568 indices clearly indicate that the composition and/or aromaticity of $WSBrC$ and $WI-MSBrC$ are
569 substantially distinct, even though they might have been mainly derived from similar sources:
570 biomass burning and coal combustion, as discussed in previous section.

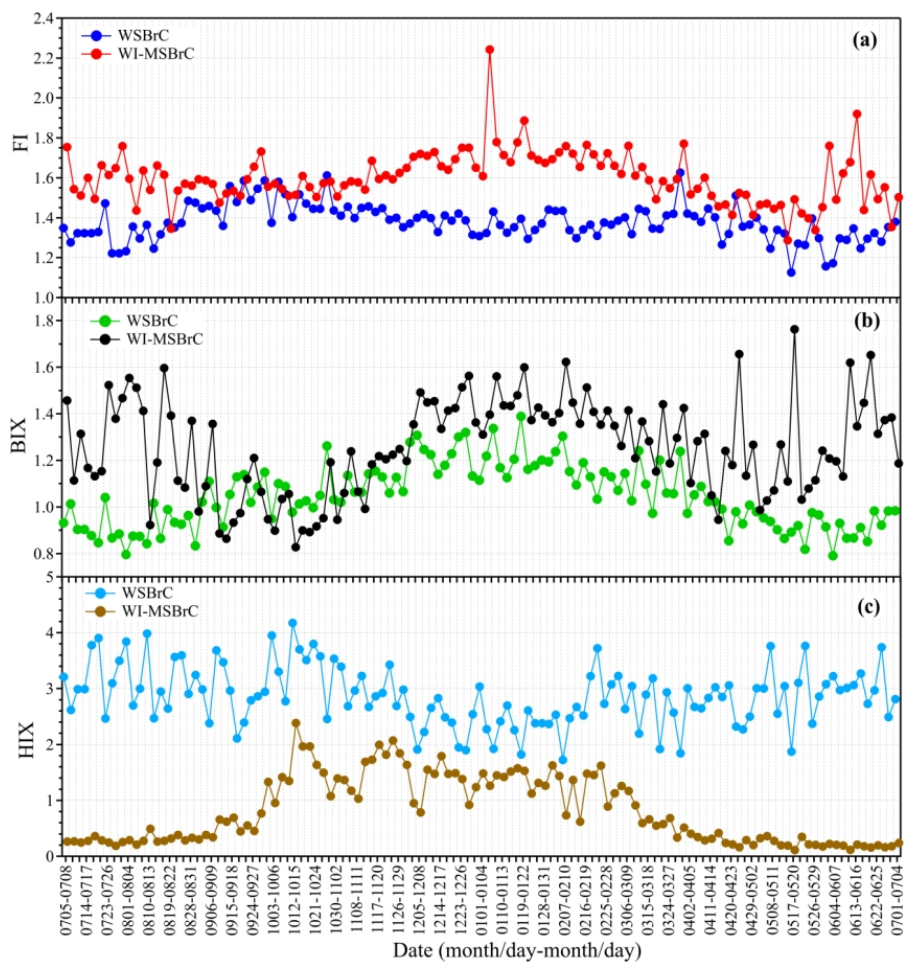
571 Average FI_{WSBrC} was found to be higher in autumn followed the similar levels in winter and
572 spring and the lowest in summer, whereas that of BIX_{WSBrC} was higher in winter followed by
573 autumn, spring and the lowest in summer (Table 1). While the averages of both $FI_{WI-MSBrC}$ and
574 $BIX_{WI-MSBrC}$ were higher in winter followed by summer, spring and the lowest in autumn (Table
575 1). Annual and seasonal averages of FI values of both $WSBrC$ and $WI-MSBrC$ were around or
576 higher than 1.4 and lower than 1.9 in Tianjin, indicating that the BrC in Tianjin was mainly derived
577 from terrestrial OM that should have largely consist of high aromatic compounds. In contrast, the
578 annual and seasonal averages of BIX of both $WSBrC$ and $WI-MSBrC$ were higher than 1.0 (Table
579 1), indicating the predominant contributions of OM from the biological (including biomass
580 burning) sources. In addition, the lowest FI_{WSBrC} and BIX_{WSBrC} values in summer and those of the
581 $FI_{WI-MSBrC}$ in spring and $BIX_{WI-MSBrC}$ in autumn suggest that the contribution from terrestrial
582 sources (e.g., coal combustion) might be less in spring and autumn and the photobleaching of OA
583 might be significant under high solar radiation in summer.

584 HIX_{WSBrC} and $HIX_{WI-MSBrC}$ were ranged from 1.72 to 4.7 with an average of 2.87 and
585 0.11-2.38 (avg. 0.81), respectively, during the campaign, which again support that both the BrC
586 components in Tianjin should have been significantly derived from biomass burning and might
587 consist highly humified and aromatic compounds. Average HIX_{WSBrC} was higher in summer
588 followed by autumn, spring and the lowest in winter (Table 1). In contrast, the average $HIX_{WI-MSBrC}$
589 $MSBrC$ was higher in winter followed by autumn, spring and the lowest in summer (Table 1). It has
590 been reported that aging processes and HIX have a significant relation (Deng et al., 2022). The
591 higher HIX_{WSBrC} and lower $HIX_{WI-MSBrC}$ in summer confirm that the BrC, which is more water-
592 soluble, was significantly produced from aromatic compounds and subjected for significant
593 atmospheric aging in summer over the Tianjin region.

594

Deleted: ave

Deleted: ave



597

598 **Figure 4.** Temporal variations in light absorption and fluorescence properties of BrC in PM_{2.5}
 599 Tianjin: (a) FI, (b) BIX, and (c) HIX.

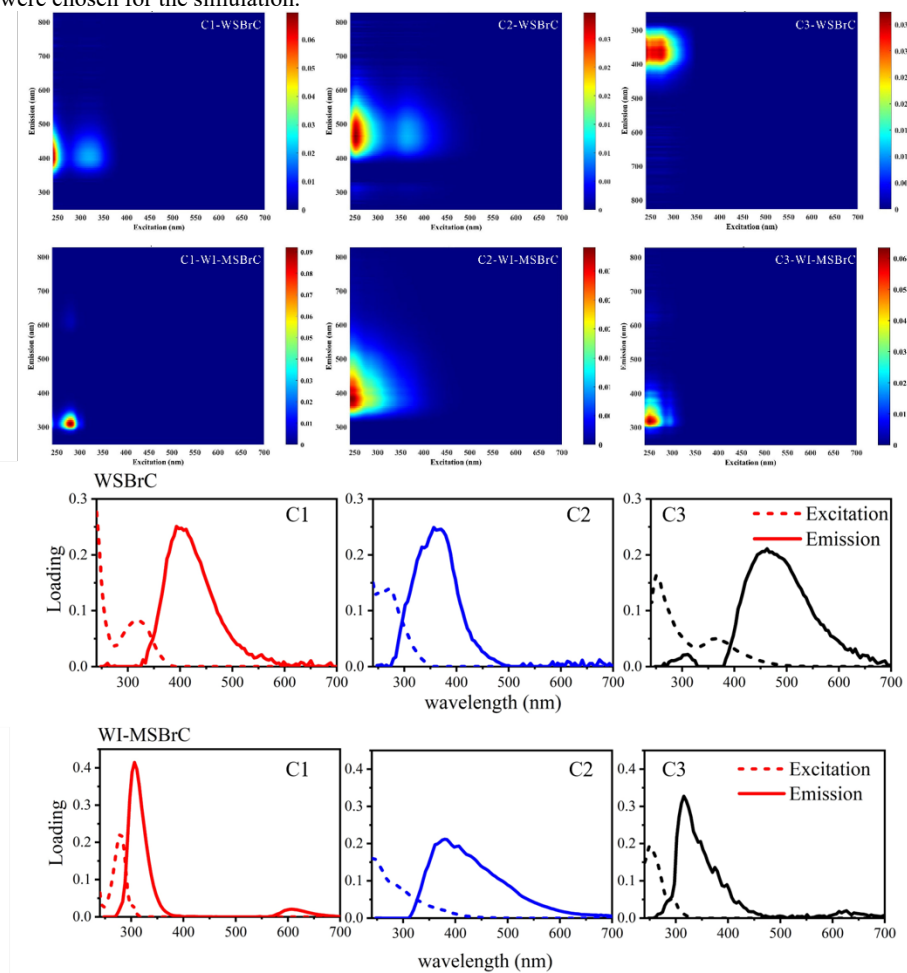
600

3.3.2 Fluorophore identification

601

602 It is well established that fluorophores with different excitation emission wavelengths can
 603 distinguish their types and sources. However, the types and sources of a large number of
 604 fluorophores have not been determined due to their complex chemical composition and sources.
 605 Here, we separated several fluorescence components from the EEM data using the parallel factor
 606 analysis (PARAFAC) model, and the results are shown in Fig. 5. The fact of the value of core
 consistency close to 100 in PARAFAC model indicates that the more the individual components

607 that are analyzed together make up 100% of the mixture, with no unexplained residues. The core
 608 consistency of PARAFAC model explained the maximum variance of 89% for WSBrc and of
 609 95% for WI-MSBrC whole data obtained during the campaign, when three independent groups
 610 were chosen for the simulation.



611
 612 **Figure 5.** Three-dimensional excitation-emission matrix of three fluorescent components with
 613 emission in WSBrc (above) and WI-MSBrC (below) obtained by PARAFAC model analysis.

614 The types of fluorophores of both WSBrc and WI-MSBrC identified in this study together
 615 with their excitation and emission wavelengths and those reported in the literature are summarized
 616 in Table 2. Among the total of three types of fluorophores obtained for WSBrc in Tianjin PM_{2.5}

617 by PARAFAC for EEMs, two showed the fluorescence characteristics similar to those of less
618 oxygenated and highly oxygenated humic-like substances (HULIS), respectively, and the third one
619 showed similar to those of protein compounds (PLOM). Fluorophore C1_{WSBrC} has a primary
620 fluorescence peak at excitation/emission (Ex/Em): <240/393 nm, and a secondary fluorescence
621 peak at Ex/Em: 318/393 nm. C1_{WSBrC} can be classified as a humus-like fluorophore because the
622 bimodal distribution of the fluorescence spectrum is usually associated with HULIS. The emission
623 wavelength of C1_{WSBrC} was closer to the UV region than that of the second peak of C2_{WSBrC},
624 indicating the existence of a small number of aromatic substances, conjugate systems and
625 nonlinear ring systems (Deng et al., 2022). C2_{WSBrC} (Ex/Em ~251, 363 nm/462 nm) was identified
626 as a common HULIS in aerosols, with higher oxidation, aromatization, molecular weight,
627 conjugation, and unsaturation due to its larger emission wavelength (Wen et al., 2021). The
628 molecular weight of the fluorophore as well as its degree of conjugation tend to increase with the
629 excitation wavelength, and such increase in size and the conjugation degree may be attributed to
630 the presence of highly aromatic conjugated structures containing heteroatoms (Chen et al., 2019).
631 Compared to C1_{WSBrC} and C2_{WSBrC}, C3_{WSBrC} also contains two peaks, with shorter wavelengths
632 (<380 nm) emission peak, which is usually associated with protein-like organic matter (PLOM)
633 such as tryptophan and tyrosine, with low aromatic properties and small molecular size (Table 2).
634

635 **Table 2.** Description and wavelength positions of PARAFAC components in this study and other
636 reports from the literature. (PLOM = protein compounds; HULIS = humic-like substances)

Category	Components	Ex(nm)	Em(nm)	Substances	References
WSBrC	C1	<240, 318	393	low-oxygenated HULIS	this study
	C2	251, 363	462	high-oxygenated HULIS	
	C3	<240, 271	356.3	PLOM, such as tryptophan and tyrosine	
WI-MSBrC	C1	<240, 279	306	PLOM, tyrosine-like	uncertain
	C2	<240	379		
	C3	251, 294	315	PLOM, tryptophan-like	
Water-soluble BrC	C1	250, 315	396	low-oxygenated HULIS	(Deng et al., 2022)
	C2	250	465	highly-oxygenated HULIS	
	C3	250	385	low-oxygenated HULIS	
	C4	250	340	PLOM, tryptophan-like	
	C5	275	305	PLOM, tyrosine-like	
WSOC	C1	240, 315	393	low-oxygenated HULIS	(Wen et al., 2021)
	C2	245, 360	476	highly-oxygenated HULIS	
	C3	<240, 290	361	PLOM, such as tryptophan and tyrosine	
	C4	275	311	PLOM, tyrosine-like	
WSM and MSM	C1	255	415	HULIS-1 component	(Chen et al., 2019)
	C2	220	340	tryptophan-like component	
	C3	255	385	HULIS-2 component	
	C4	210	300	tyrosine-like component	
	C5	250	355	amino acid-like component	
WSOC	C1	245	410	HULIS, photodegradation of macromolecules	(Xie et al., 2020)
	C2	235	398	HULIS, aromatic and saturated compounds were presented	
	C3	250, 360	466	humic-like chromophores, more aromatic and consisted of more unsaturated compounds produced by condensation reactions	
	C4	250, 285	432	terrestrial humic-like chromophore	
MSOC	C5	<235	430	terrestrial humic-like substance, photochemical product	
	C6	275	408	low oxidation humic-like	
	C7	235, 275	372	protein-like chromophore	
	C8	260, 310	364	protein-like (tryptophan-like), may be related to PAHs	

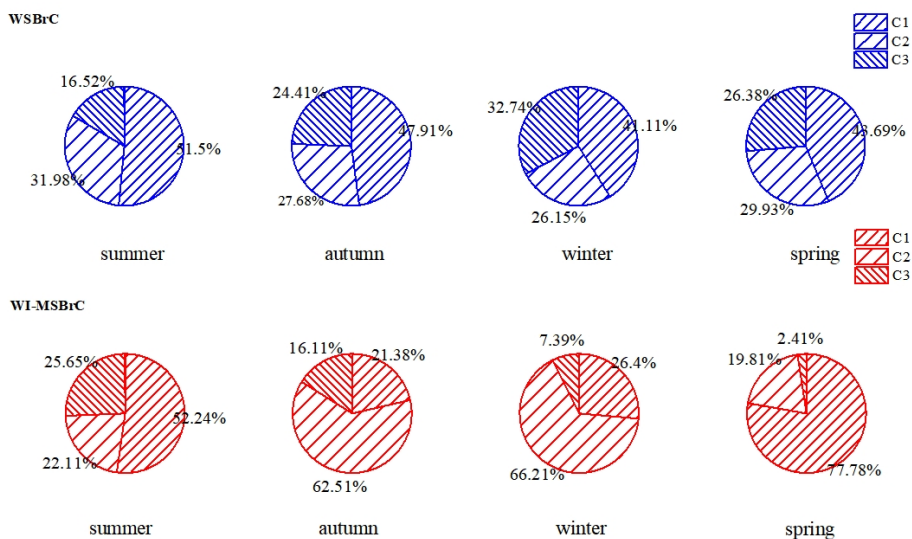
637 However, WI-MSBrC fluorophore C1_{WI-MSBrC} might be tyrosine-like substance. C2_{WI-MSBrC}
638 is not quite certain and could be either HULIS or PLOM, because its emission wavelength <380
639

640 nm generally fits the profile of PLOM, but it is also close to the emission wavelength of HULIS.
 641 While C3_{WI-MSBrC} is a tryptophan-like substance, which was reported to contain less aromatic and
 642 small molecular weight compounds. In general, phenols contribute significantly to C3_{WI-MSBrC}
 643 fluorophore as they are the products of incomplete pyrolysis of lignin and cellulose and are used
 644 as indicators of biomass burning (Wen et al., 2021). Therefore, WI-MSBrC fluorophores of all
 645 samples in this study can be classified as mainly PLOM.

646 The percent contributions of each fluorophore to WSB_{rC} and WI-MSBrC in PM_{2.5} in Tianjin
 647 in each season are shown in Fig. 6. The compositions of WSB_{rC} and WI-BrC clearly imply that
 648 the former contained more HULIS, whereas the later consist mostly of PLOM, and also indicate
 649 that most of the fluorophores of protein-like substances could dissolve in organic solvent, rather
 650 than in water.

651 According to the excitation emission wavelength, we classified the fluorescence component
 652 of WI-MSBrC substance as PLOM, but the correlation between their fluorescence intensity and
 653 BIX ($R = 0.66, p < 0.05$) was very small, far lower than that of WSB_{rC} substance and BIX ($R =$
 654 $0.59, p < 0.05$). On the contrary, the correlation between their fluorescence intensity and HIX (R
 655 $= 0.74, p < 0.05$) was much higher than that of WSB_{rC} ($R = -0.10, p < 0.05$). Although PLOM
 656 may be associated with some polycyclic aromatic hydrocarbons (PAHs) or phenols from fossil
 657 fuel combustion and biomass burning, especially in urban aerosols, the correlation is puzzling.

658



659

660 **Figure 6.** Relative abundances of the chromophores of the WSB_{rC} and WI-MSBrC in PM_{2.5}
 661 from Tianjin.

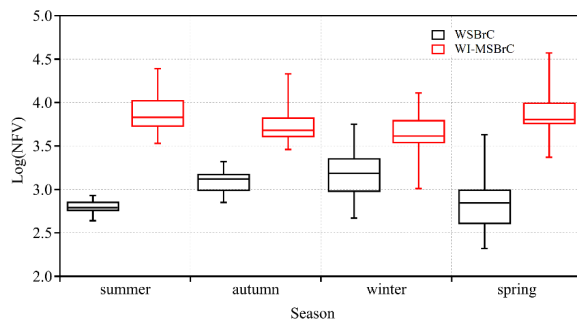
662 On average, the humic-like fluorophores together contributed more than 60% to the
 663 fluorescence intensity in WSB_{rC}, suggesting that humic-like fluorophores played a dominant role
 664 in fluorescence properties of WSB_{rC} in Tianjin. Generally, the low-oxygenated fluorophores
 665 C1_{WSBrC} made considerable contributions in each season. While C2_{WSBrC}, highly oxygenated

666 HULIS, has a greater relative contribution in summer, which might be due to the strong solar
667 radiation in summer. In contrast, in WI-MSBrC, the average contribution of PLOM to fluorescence
668 intensity was higher than 70% in spring (80.2%) and summer (77.9%), but C2_{WI-MSBrC} component
669 dominated in winter and autumn. This indicated that biological activities increased in spring and
670 summer and the relative abundance of bioaerosols might be higher during that period.

671 3.4 Potential sources of BrC

672 To further explore the potential sources of BrC, correlations of FV with chemical components
673 and light absorption of PM_{2.5} were examined. The sum of FVs of WSB_rC and WI-MSBrC
674 (FV_{S(WSB_rC+WI-MSBrC)}) showed a significant correlation with secondary OC (SOC) in autumn (R =
675 0.90, $p < 0.05$) and winter (R = 0.67, $p < 0.05$). Furthermore, the correlation between FV<sub>S(WSB_rC+WI-
676 MSBrC)</sub> and EC in each season was insignificant. Such relations suggest that the secondary
677 formation processes should have been played an important role in controlling the loadings of BrC
678 in autumn and winter as well. A good correlation between FV and Abs₃₆₅ of both WSB_rC and WI-
679 MSBrC was found in all seasons except winter, which indicates that most light-absorbing materials
680 would also have significant fluorescence characteristics.

681 The relative contents of different chromophores in different polar extracts depend on their
682 sources and varied significantly. The results showed that the NFVs of WSB_rC were lower than
683 those the WI-MSBrC and were different from season to season in Tianjin (Fig. 7). Recently, it has
684 been reported that the aerosols derived from biomass burning and coal combustion exhibit the
685 highest NFV values, while SOA show the lowest NFV values (Chen et al., 2020). NFV in all
686 samples studied in Tianjin during 2018–2019 was very similar to that of primary emissions and
687 higher than that of secondary aerosols. Such result reveal that the fluorophores in the Tianjin PM_{2.5}
688 might mainly be derived from a primary combustion sources as well. In addition, the NFVs of the
689 Tianjin PM_{2.5} were higher in winter than in summer, which is likely and can be attributed to the
690 photolysis of chromophores in summer. In addition, NFV of WI-MSBrC was much higher than
691 that in WSB_rC, which indicate that fluorescence contribution of fluorophores was abundant in WI-
692 MSBrC than in the WSB_rC.



693

694 **Figure 7.** The normalized fluorescence volumes (NFVs) of the WSB_rC and WI-MSBrC of PM_{2.5}
695 from Tianjin, North China.

696

697 **4. Summary and Conclusions**

698 This study presents the temporal variations in light absorption and fluorescence properties of
699 water-soluble BrC (WSBrC) and the water-insoluble but MeOH-soluble BrC (WI-MSBrC) in
700 PM_{2.5} collected from Tianjin, North China during July 5, 2018 – July 5, 2019. Light absorption
701 properties of WSBrC and WI-MSBrC in Tianjin were investigated and found to be distinct from
702 season to season, which was lower in spring and summer, compared with that in autumn and
703 winter. The AAE of WI-MSBrC was comparable with that of WSBrC. The mass absorption
704 efficiency of WSBrC and WI-MSBrC (MAE₃₆₅) exhibited distinct seasonal variations, which was
705 higher in winter and lower in summer and autumn. Biologically derived or secondary BrC and/or
706 its photobleaching might be the reasons for the lower MAE₃₆₅ values in summer and autumn. The
707 light absorption of both WSBrC and WI-MSBrC in the range of 300–400 nm to that in the whole
708 range (300–700 nm) was ~40%, indicating that BrC in the UV-Vis range plays an important role
709 in climate warming. In addition, based on PARAFAC analysis model, EEM data were
710 comprehensively analyzed to identify the types and abundance of different fluorophores, and
711 obtained three types of the fluorophores: low-oxygenated HULIS, high-oxygenated HULIS and
712 protein-like compound (PLOM). The correlation between BrC optical properties and aerosol
713 chemical composition indicated that biomass burning, and fossil fuel (mainly coal) combustion
714 significantly contributed to BrC content in winter, while primary biological emission and
715 subsequent aging significantly contributed to the BrC content in summer. These results illustrated
716 the light absorption properties of BrC in metropolis aerosols and emphasized its significant
717 contribution to radiative forcing.

718 **Declaration of competing interest**

719 The authors declare no competing interest in this paper.

720 **Data Availability Statement**

721 The data used in this study can be found online at <https://doi.org/10.5281/zenodo.7316371> (Dong
722 et al., 2022), and at <https://doi.org/10.5281/zenodo.5140861> (Dong et al., 2021).

723 **Supplement.**

724 The supplement related to this article is available online at:

725 **Acknowledgments**

726 This work was supported in part by National Natural Science Foundation of China (Grant No.
727 41775120 and 42277090) & National Key Research and Development Plan (Grant No.
728 2017YFC0212700), China. The author also thanks to Mr. Yunting Xiao's help for writing a code
729 to calculate the SFE.

730 **Author contribution**

731 ZD and CMP conceptualized this study. ZD and PL conducted the sampling. ZD conducted the

732 chemical analyses, interpreted the data and wrote the manuscript. CMP supervised the research
733 and acquired the funding for this study. XZ, ZXY and ZXM administrated the project. CMP, ZX,
734 DJ, PF and CQL contributed in discussing the results and review and editing the manuscript.

735 References

- 736 Andreae, M. O., and Gelas' er, A.: Black carbon or brown carbon? The nature of light-absorbing carbonaceous
737 aerosols, *Atmospheric Chemistry and Physics*, 6, 3131–3148, www.atmos-chem-phys.net/6/3131/2006/, 2006.
- 738 Baduel, C., Voisin, D., and Jaffrezo, J. L.: Comparison of analytical methods for Humic Like Substances (HULIS)
739 measurements in atmospheric particles, *Atmospheric Chemistry and Physics*, 9, 5949–5962, 10.5194/acp-9-5949-
740 2009, 2009.
- 741 Battin, T. J.: Dissolved organic matter and its optical properties in a blackwater tributary of the upper Orinoco river,
742 Venezuela, *Organic Geochemistry*, 28, 561–569, [https://doi.org/10.1016/S0146-6380\(98\)00028-X](https://doi.org/10.1016/S0146-6380(98)00028-X), 1998.
- 743 Birdwell, J. E., and Engel, A. S.: Characterization of dissolved organic matter in cave and spring waters using UV-
744 Vis absorbance and fluorescence spectroscopy, *Org Geochem*, 41, 270–280, 10.1016/j.orggeochem.2009.11.002,
745 2010.
- 746 Bond, T. C., and Bergstrom, R. W.: Light absorption by carbonaceous particles: An investigative review, *Aerosol
747 Science and Technology*, 40, 27–67, 10.1080/02786820500421521, 2006.
- 748 Brown, H., Liu, X., Pokhrel, R., Murphy, S., Lu, Z., Saleh, R., Mielonen, T., Kokkola, H., Bergman, T., Myhre, G.,
749 Skeie, R. B., Watson-Paris, D., Stier, P., Johnson, B., Bellouin, N., Schulz, M., Vakkari, V., Beukes, J. P., van Zyl,
750 P. G., Liu, S., and Chand, D.: Biomass burning aerosols in most climate models are too absorbing, *Nature
751 Communications*, 12, 277, 10.1038/s41467-020-20482-9, 2021.
- 752 Cao, T., Li, M., Xu, C., Song, J., Fan, X., Li, J., Jia, W., and Peng, P.: Technical note: Identification of chemical
753 composition and source of fluorescent components in atmospheric water-soluble brown carbon by excitation-
754 emission matrix with parallel factor analysis: Potential limitation and application, *Atmospheric Chemistry and
755 Physics Discussions*, 2022, 1–41, 10.5194/acp-2022-676, 2022.
- 756 Chen, Q., Fumikazu, I., Hayato, H., Daichi, A., and Michihiro, M.: Chemical structural characteristics of HULIS
757 and other fractionated organic matter in urban aerosols: Results from mass spectral and FT-IR analysis,
758 *Environmental Science & Technology*, 50, 1721–1730, 10.1021/acs.est.5b05277, 2016a.
- 759 Chen, Q., Miyazaki, Y., Kawamura, K., Matsumoto, K., Coburn, S., Volkamer, R., Iwamoto, Y., Kagami, S., Deng,
760 Y., Ogawa, S., Ramasamy, S., Kato, S., Ida, A., Kajii, Y., and Mochida, M.: Characterization of chromophoric
761 water-soluble organic matter in urban, forest, and marine aerosols by HR-ToF-AMS analysis and excitation-
762 emission matrix spectroscopy, *Environmental Science & Technology*, 50, 10351–10360, 10.1021/acs.est.6b01643,
763 2016b.
- 764 Chen, Q., Mu, Z., Song, W., Wang, Y., Yang, Z., Zhang, L., and Zhang, Y.-L.: Size-resolved characterization of the
765 chromophores in atmospheric particulate matter from a typical coal-burning city in China, *Journal of Geophysical
766 Research: Atmospheres*, 124, 10546–10563, <https://doi.org/10.1029/2019JD031149>, 2019.
- 767 Chen, Q., Li, J., Hua, X., Jiang, X., Mu, Z., Wang, M., Wang, J., Shan, M., Yang, X., Fan, X., Song, J., Wang, Y.,
768 Guan, D., and Du, L.: Identification of species and sources of atmospheric chromophores by fluorescence excitation-
769 emission matrix with parallel factor analysis, *Science of the Total Environment*, 718, 137322,
770 10.1016/j.scitotenv.2020.137322, 2020.
- 771 Chen, Q. C., Ikemori, F., and Mochida, M.: Light Absorption and Excitation-Emission Fluorescence of Urban
772 Organic Aerosol Components and Their Relationship to Chemical Structure, *Environ Sci Technol*, 50, 10859–10868,
773 10.1021/acs.est.6b02541, 2016c.
- 774 Choudhary, V., Rajput, P., and Gupta, T.: Absorption properties and forcing efficiency of light-absorbing water-
775 soluble organic aerosols: Seasonal and spatial variability, *Environ Pollut*, 272, ARTN 115932
776 10.1016/j.envpol.2020.115932, 2021.
- 777 Coble, P. G.: Marine optical biogeochemistry: The chemistry of ocean color, *Chem Rev*, 107, 402–418,
778 10.1021/cr050350+, 2007.
- 779 Corbin, J. C., Czech, H., Massabò, D., de Mongeot, F. B., Jakobi, G., Liu, F., Lobo, P., Mennucci, C., Mensah, A.
780 A., Orasche, J., Pieber, S. M., Prévôt, A. S. H., Stengel, B., Tay, L. L., Zanatta, M., Zimmermann, R., El Haddad, I.,
781 and Gysel, M.: Infrared-absorbing carbonaceous tar can dominate light absorption by marine-engine exhaust, *npj
782 Climate and Atmospheric Science*, 2, 12, 10.1038/s41612-019-0069-5, 2019.

Field Code Changed

783 Deng, J., Ma, H., Wang, X., Zhong, S., Zhang, Z., Zhu, J., Fan, Y., Hu, W., Wu, L., Xiaodong, L., Ren, L., Pavuluri,
784 C. M., Pan, X., Sun, Y., Wang, Z., Kawamura, K., and Fu, P.: Measurement Report: Optical properties and sources
785 of water-soluble brown carbon in Tianjin, North China: insights from organic molecular compositions, *Atmospheric
786 Chemistry and Physics*, 22, 6449-6470, 10.5194/acp-2021-1045, 2022.

787 Diggs, D. L., Huderson, A. C., Harris, K. L., Myers, J. N., Banks, L. D., Rekhadevi, P. V., Niaz, M. S., and Ramesh,
788 A.: Polycyclic aromatic hydrocarbons and digestive tract cancers: a perspective, *Journal of Environmental Science
789 and Health, Part C*, 29, 324-357, 10.1080/10590501.2011.629974, 2011.

790 Dong, Z., Pavuluri, C. M., Xu, Z., Wang, Y., Li, P., Fu, P., and Liu, C. Q.: Measurement report: Chemical
791 components and ¹³C and ¹⁵N isotope ratios of fine aerosols over Tianjin, North China: year-round observations,
792 *Atmospheric Chemistry and Physics*, 23, 2119-2143, 10.5194/acp-23-2119-2023, 2023a.

793 Dong, Z. C., Pavuluri, C. M., Xu, Z. J., Wang, Y., Li, P. S., Fu, P. Q., and Liu, C. Q.: Year-round observations of
794 bulk components and ¹³C and ¹⁵N isotope ratios of fine aerosols at Tianjin, North China – Data set. 2021.

795 Dong, Z. C., Pavuluri, C. M., Li, P. S., Xu, Z. J., Deng, J. J., Zhao, X. Y., and Zhao, X. M.: Year-round observations
796 of the optical properties of brown carbon in fine aerosols at Tianjin, North China – Data set. 2022.

797 Dong, Z. C., Pavuluri, C. M., Xu, Z. J., Wang, Y., Li, P. S., Fu, P. Q., and Liu, C. Q.: Measurement report:
798 Chemical components and
799 C and
800 N isotoperatios of fine aerosols over Tianjin, North China: year-round observations, *Atmos Chem Phys*, 23, 2119-
801 2143, 10.5194/acp-23-2119-2023, 2023b.

802 Fan, X. J., Wei, S. Y., Zhu, M. B., Song, J. Z., and Peng, P. A.: Comprehensive characterization of humic-like
803 substances in smoke PM
804 emitted from the combustion of biomass materials and fossil fuels, *Atmos Chem Phys*, 16, 13321-13340,
805 10.5194/acp-16-13321-2016, 2016.

806 Feng, Y., Ramanathan, V., and Kotamarthi, V. R.: Brown carbon: a significant atmospheric absorber of solar
807 radiation?, *Atmospheric Chemistry and Physics Discussions*, 10.5194/acpd-13-2795-2013, 2013.

808 Gao yan, and Zhang, y.: Formation and photochemical investigation of brown carbon by hydroxyacetone reactions
809 with glycine and ammonium sulfate, *Royal Society of Chemistry Advances*, 8, 20719-20725,
810 10.1039/C8RA02019A, 2018.

811 Gu, Q., and Kenny, J. E.: Improvement of inner filter effect correction based on determination of effective geometric
812 parameters using a conventional fluorimeter, *Analytical Chemistry*, 81, 420-426, 10.1021/ac801676j, 2009.

813 Hecobian, A., Zhang, X., Zheng, M., Frank, N., Edgerton, E. S., and Weber, R. J.: Water-Soluble Organic Aerosol
814 material and the light-absorption characteristics of aqueous extracts measured over the Southeastern United States,
815 *Atmospheric Chemistry and Physics*, 10, 5965-5977, 10.5194/acp-10-5965-2010, 2010.

816 Hems, R. F., Schnitzler, E. G., Liu-Kang, C., Cappa, C. D., and Abbatt, J. P. D.: Aging of atmospheric brown carbon
817 aerosol, *ACS Earth and Space Chemistry*, 5, 722-748, 10.1021/acsearthspacechem.0c00346, 2021.

818 Hoffer, A., Gelencsér, A., Guyon, P., Kiss, G., Schmid, O., Frank, G. P., Artaxo, P., and Andreae, M. O.: Optical
819 properties of humic-like substances (HULIS) in biomass-burning aerosols, *Atmospheric Chemistry and Physics*, 6,
820 3563-3570, 10.5194/acp-6-3563-2006, 2006.

821 Huang, R. J., Yang, L., Cao, J., Chen, Y., Chen, Q., Li, Y., Duan, J., Zhu, C., Dai, W., Wang, K., Lin, C., Ni, H.,
822 Corbin, J. C., Wu, Y., Zhang, R., Tie, X., Hoffmann, T., O'Dowd, C., and Dusek, U.: Brown carbon aerosol in urban
823 Xi'an, Northwest China: The composition and light absorption properties, *Environmental Science & Technology*,
824 52, 6825-6833, 10.1021/acs.est.8b02386, 2018.

825 Huang, R. J., Yang, L., Shen, J., Yuan, W., Gong, Y., Guo, J., Cao, W., Duan, J., Ni, H., Zhu, C., Dai, W., Li, Y.,
826 Chen, Y., Chen, Q., Wu, Y., Zhang, R., Dusek, U., O'Dowd, C., and Hoffmann, T.: Water-insoluble organics
827 dominate brown carbon in wintertime urban aerosol of China: Chemical characteristics and optical properties,
828 *Environmental Science & Technology*, 54, 7836-7847, 10.1021/acs.est.0c01149, 2020.

829 Jo, D. S., Park, R. J., Lee, S., Kim, S. W., and Zhang, X.: A global simulation of brown carbon: implications for
830 photochemistry and direct radiative effect, *Atmospheric Chemistry and Physics*, 16, 3413-3432, 10.5194/acp-16-
831 3413-2016, 2016.

832 Kasthuriarachchi, N. Y., Rivellini, L.-H., Chen, X., Li, Y. J., and Lee, A. K. Y.: Effect of relative humidity on
833 secondary brown carbon formation in aqueous droplets, *Environmental Science & Technology*, 54, 13207-13216,
834 10.1021/acs.est.0c01239, 2020.

835 Lack, D. A., Bahreni, R., Langridge, J. M., Gilman, J. B., and Middlebrook, A. M.: Brown carbon absorption linked
836 to organic mass tracers in biomass burning particles, *Atmospheric Chemistry and Physics*, 13, 2415-2422,
837 10.5194/acp-13-2415-2013, 2013.

838 Laskin, A., Laskin, J., and Nizkorodov, S. A.: Chemistry of Atmospheric Brown Carbon, *Chem Rev*, 115, 4335-
839 4382, 10.1021/cr5006167, 2015a.

840 Laskin, A., Laskin, J., and Nizkorodov, S. A.: Chemistry of atmospheric brown carbon, *Chemical Reviews*, 115,
841 4335-4382, 10.1021/cr5006167, 2015b.

842 Lawaetz, A. J., and Stedmon, C. A.: Fluorescence intensity calibration using the Raman scatter peak of water,
843 *Applied Spectroscopy*, 63, 936-940, 10.1366/000370209788964548, 2009.

844 Lee, H. J., Laskin, A., Laskin, J., and Nizkorodov, S. A.: Excitation-Emission Spectra and Fluorescence Quantum
845 Yields for Fresh and Aged Biogenic Secondary Organic Aerosols, *Environ Sci Technol*, 47, 5763-5770,
846 10.1021/es400644c, 2013.

847 Lesworth, T., Baker, A. R., and Jickells, T.: Aerosol organic nitrogen over the remote Atlantic Ocean, *Atmospheric*
848 *Environment*, 44, 1887-1893, <https://doi.org/10.1016/j.atmosenv.2010.02.021>, 2010.

849 Li, C., He, Q., Hettiyadura, A. P. S., Käfer, U., Shmul, G., Meidan, D., Zimmermann, R., Brown, S. S., George, C.,
850 Laskin, A., and Rudich, Y.: Formation of secondary brown carbon in biomass burning aerosol proxies through NO₃
851 radical reactions, *Environmental Science & Technology*, 54, 1395-1405, 10.1021/acs.est.9b05641, 2020a.

852 Li, J., Zhang, Q., Wang, G., Li, J., Wu, C., Liu, L., Wang, J., Jiang, W., Li, L., Ho, K. F., and Cao, J.: Optical
853 properties and molecular compositions of water-soluble and water-insoluble brown carbon (BrC) aerosols in
854 northwest China, *Atmospheric Chemistry and Physics*, 20, 4889-4904, 10.5194/acp-20-4889-2020, 2020b.

855 Li, S., Zhu, M., Yang, W. Q., Tang, M. J., Huang, X. L., Yu, Y. G., Fang, H., Yu, X., Yu, Q. Q., Fu, X. X., Song,
856 W., Zhang, Y. L., Bi, X. H., and Wang, X. M.: Filter-based measurement of light absorption by brown carbon in
857 PM_{2.5} in a megacity in South China, *Science of the Total Environment*, 633, 1360-1369,
858 10.1016/j.scitotenv.2018.03.235, 2018.

859 Li, X., Fu, P., Tripathee, L., Yan, F., Hu, Z., Yu, F., Chen, Q., Li, J., Chen, Q., Cao, J., and Kang, S.: Molecular
860 compositions, optical properties, and implications of dissolved brown carbon in snow/ice on the Tibetan Plateau
861 glaciers, *Environment International*, 164, 107276, <https://doi.org/10.1016/j.envint.2022.107276>, 2022.

862 Liakakou, E., Kaskaoutis, D. G., Grivas, G., Stavroulas, I., Tsagkaraki, M., Paraskevopoulou, D., Bougiatioti, A.,
863 Dumka, U. C., Gerasopoulos, E., and Mihalopoulos, N.: Long-term brown carbon spectral characteristics in a
864 Mediterranean city (Athens), *Sci Total Environ*, 708, 135019, 10.1016/j.scitotenv.2019.135019, 2020.

865 Lin, G., Penner, J. E., Flanner, M. G., Sillman, S., Xu, L., and Zhou, C.: Radiative forcing of organic aerosol in the
866 atmosphere and on snow: Effects of SOA and brown carbon, *Journal of Geophysical Research: Atmospheres*, 119,
867 7453-7476, 10.1002/2013jd021186, 2014.

868 Lin, P., Bluvshstein, N., Rudich, Y., Nizkorodov, S. A., Laskin, J., and Laskin, A.: Molecular Chemistry of
869 Atmospheric Brown Carbon Inferred from a Nationwide Biomass Burning Event, *Environ Sci Technol*, 51, 11561-
870 11570, 10.1021/acs.est.7b02276, 2017.

871 Liu, J., Bergin, M., Guo, H., King, L., Kotra, N., Edgerton, E., and Weber, R. J.: Size-resolved measurements of
872 brown carbon in water and methanol extracts and estimates of their contribution to ambient fine-particle light
873 absorption, *Atmospheric Chemistry and Physics*, 13, 12389-12404, 10.5194/acp-13-12389-2013, 2013.

874 McKnight, D. M., Boyer, E. W., Westerhoff, P. K., Doran, P. T., Kulbe, T., and Andersen, D. T.:
875 Spectrofluorometric Characterization of Dissolved Organic Matter for Indication of Precursor Organic Material and
876 Aromaticity, *Limnology and Oceanography*, 46, 38-48, 2001.

877 Murphy, K. R., Stedmon, C. A., Graeber, D., and Bro, R.: Fluorescence spectroscopy and multi-way techniques.
878 PARAFAC, *Analytical Methods*, 5, 6557-6566, 10.1039/C3AY41160E, 2013.

879 Park, R. J., Kim, M. J., Jeong, J. I., Youn, D., and Kim, S.: A contribution of brown carbon aerosol to the aerosol
880 light absorption and its radiative forcing in East Asia, *Atmospheric Environment*, 44, 1414-1421,
881 10.1016/j.atmosenv.2010.01.042, 2010.

882 Peters, S., Talaska, G., Jonsson, B. A., Kromhout, H., and Vermeulen, R.: Polycyclic aromatic hydrocarbon
883 exposure, urinary mutagenicity, and DNA adducts in rubber manufacturing workers, *Cancer Epidemiol Biomarkers*
884 *Prev*, 17, 1452-1459, 10.1158/1055-9965.EPI-07-2777, 2008.

885 Qin, J., Zhang, L., Zhou, X., Duan, J., Mu, S., Xiao, K., Hu, J., and Tan, J.: Fluorescence fingerprinting properties
886 for exploring water-soluble organic compounds in PM_{2.5} in an industrial city of northwest China, *Atmospheric*
887 *Environment*, 184, 203-211, <https://doi.org/10.1016/j.atmosenv.2018.04.049>, 2018.

888 Rizzo, L. V., Correia, A. L., Artaxo, P., Procópio, A. S., and Andreae, M. O.: Spectral dependence of aerosol light
889 absorption over the Amazon Basin, *Atmospheric Chemistry and Physics*, 11, 8899-8912, 10.5194/acp-11-8899-
890 2011, 2011.

891 Rizzo, L. V., Artaxo, P., Müller, T., Wiedensohler, A., Paixão, M., Cirino, G. G., Arana, A., Swietlicki, E., Roldin,
892 P., Fors, E. O., Wiedemann, K. T., Leal, L. S. M., and Kulmala, M.: Long term measurements of aerosol optical

893 properties at a primary forest site in Amazonia, *Atmos. Chem. Phys.*, 13, 2391-2413, 10.5194/acp-13-2391-2013,
894 2013.

895 Saleh, R.: From Measurements to Models: Toward Accurate Representation of Brown Carbon in Climate
896 Calculations, *Current Pollution Reports*, 6, 90-104, 10.1007/s40726-020-00139-3, 2020.

897 Shamjad, P. M., Tripathi, S. N., Thamban, N. M., and Vreeland, H.: Refractive Index and Absorption Attribution of
898 Highly Absorbing Brown Carbon Aerosols from an Urban Indian City-Kanpur, *Sci Rep-Uk*, 6, 10.1038/srep37735,
899 2016.

900 Shetty, N. J., Pandey, A., Baker, S., Hao, W. M., and Chakrabarty, R. K.: Measuring light absorption by freshly
901 emitted organic aerosols: optical artifacts in traditional solvent-extraction-based methods, *Atmos. Chem. Phys.*, 19,
902 8817-8830, 10.5194/acp-19-8817-2019, 2019.

903 Sun, J., Zhi, G., Hitznerberger, R., Chen, Y., Tian, C., Zhang, Y., Feng, Y., Cheng, M., Zhang, Y., Cai, J., Chen, F.,
904 Qiu, Y., Jiang, Z., Li, J., Zhang, G., and Mo, Y.: Emission factors and light absorption properties of brown carbon
905 from household coal combustion in China, *Atmos. Chem. Phys.*, 17, 4769-4780, 10.5194/acp-17-4769-2017, 2017.

906 Tang, J., Li, J., Mo, Y., Safaei Khorram, M., Chen, Y., Tang, J., Zhang, Y., Song, J., and Zhang, G.: Light
907 absorption and emissions inventory of humic-like substances from simulated rainforest biomass burning in
908 Southeast Asia, *Environmental Pollution*, 262, 114266, <https://doi.org/10.1016/j.envpol.2020.114266>, 2020.

909 Wang, D., Shen, Z., Zhang, Q., Lei, Y., Zhang, T., Huang, S., Sun, J., Xu, H., and Cao, J.: Winter brown carbon
910 over six of China's megacities: light absorption, molecular characterization, and improved source apportionment
911 revealed by multilayer perceptron neural network, *Atmospheric Chemistry and Physics*, 22, 14893-14904,
912 10.5194/acp-22-14893-2022, 2022a.

913 Wang, Q. Q., Zhou, Y. Y., Ma, N., Zhu, Y., Zhao, X. C., Zhu, S. W., Tao, J. C., Hong, J., Wu, W. J., Cheng, Y. F.,
914 and Su, H.: Review of brown carbon aerosols in China: Pollution level, optical properties, and emissions, *Journal of*
915 *Geophysical Research: Atmospheres*, 127, 10.1029/2021JD035473, 2022b.

916 Wang, Y., Pavuluri, C. M., Fu, P., Li, P., Dong, Z., Xu, Z., Ren, H., Fan, Y., Li, L., Zhang, Y.-L., and Liu, C.-Q.:
917 Characterization of Secondary Organic Aerosol Tracers over Tianjin, North China during Summer to Autumn, *ACS*
918 *Earth and Space Chemistry*, 3, 2339-2352, 10.1021/acsearthspacechem.9b00170, 2019.

919 Wen, H., Zhou, Y., Xu, X., Wang, T., Chen, Q., Li, W., Wang, Z., Huang, Z., Zhou, T., Shi, J., Bi, J., Ji,
920 M., and Wang, X.: Water-soluble brown carbon in atmospheric aerosols along the transport pathway of Asian dust:
921 Optical properties, chemical compositions, and potential sources, *Science of the Total Environment*, 789, 147971,
922 10.1016/j.scitotenv.2021.147971, 2021.

923 Wu, G., Fu, P., Ram, K., Song, J., Chen, Q., Kawamura, K., Wan, X., Kang, S., Wang, X., Laskin, A., and Cong, Z.:
924 Fluorescence characteristics of water-soluble organic carbon in atmospheric aerosol, *Environmental Pollution*, 268,
925 115906, 10.1016/j.envpol.2020.115906, 2021a.

926 Wu, G. M., Fu, P. Q., Ram, K., Song, J. Z., Chen, Q. C., Kawamura, K., Wan, X., Kang, S. C., Wang, X. P., Laskin,
927 A., and Cong, Z. Y.: Fluorescence characteristics of water-soluble organic carbon in atmospheric aerosol, *Environ*
928 *Pollut*, 268, ARTN 115906
929 10.1016/j.envpol.2020.115906, 2021b.

930 Xie, X., Chen, Y., Nie, D., Liu, Y., Liu, Y., Lei, R., Zhao, X., Li, H., and Ge, X.: Light-absorbing and fluorescent
931 properties of atmospheric brown carbon: A case study in Nanjing, China, *Chemosphere*, 251, 126350,
932 10.1016/j.chemosphere.2020.126350, 2020.

933 Yan, J., Wang, X., Gong, P., Wang, C., and Cong, Z.: Review of brown carbon aerosols: Recent progress and
934 perspectives, *Sci Total Environ*, 634, 1475-1485, 10.1016/j.scitotenv.2018.04.083, 2018.

935 Yu, H., Liang, H., Qu, F., Han, Z. S., Shao, S., Chang, H., and Li, G.: Impact of dataset diversity on accuracy and
936 sensitivity of parallel factor analysis model of dissolved organic matter fluorescence excitation-emission matrix,
937 *Scientific Reports*, 5, 10207, 10.1038/srep10207, 2015.

938 Yue, S., Zhu, J., Chen, S., Xie, Q., Li, W., Li, L., Ren, H., Sihui, S., Ping, L., Ma, H., Fan, Y., Cheng, B., Wu, L.,
939 Deng, J., Hu, W., Ren, L., Lianfang, W., Zhao, W., Tian, Y., and Fu, P.: Brown carbon from biomass burning
940 imposes strong circum-Arctic warming, *One Earth*, 5, 293-304, 10.1016/j.oneear.2022.02.006, 2022.

941 Yue, S. Y., Bikkina, S., Gao, M., Barrie, L., Kawamura, K., and Fu, P. Q.: Sources and Radiative Absorption of
942 Water-Soluble Brown Carbon in the High Arctic Atmosphere, *Geophys Res Lett*, 46, 14881-14891,
943 10.1029/2019gl085318, 2019.

944 Zhan, Y., Li, J., Tsona, N. T., Chen, B., Yan, C., George, C., and Du, L.: Seasonal variation of water-soluble brown
945 carbon in Qingdao, China: Impacts from marine and terrestrial emissions, *Environmental Research*, 212, 113144,
946 <https://doi.org/10.1016/j.envres.2022.113144>, 2022.

947 Zhang, Q., Jimenez, J. L., Canagaratna, M. R., Ulbrich, I. M., Ng, N. L., Worsnop, D. R., and Sun, Y.:
948 Understanding atmospheric organic aerosols via factor analysis of aerosol mass spectrometry: a review, *Analytical*
949 *Chemistry and Bioanalytical Chemistry*, 401, 3045-3067, 10.1007/s00216-011-5355-y, 2011.
950 Zhang, Q., Shen, Z., Zhang, T., Kong, S., Lei, Y., Wang, Q., Tao, J., Zhang, R., Wei, P., Wei, C., Cui, S., Cheng, T.,
951 Ho, S. S. H., Li, Z., Xu, H., and Cao, J.: Spatial distribution and sources of winter black carbon and brown carbon in
952 six Chinese megacities, *Science of The Total Environment*, 762, 143075,
953 <https://doi.org/10.1016/j.scitotenv.2020.143075>, 2021.
954 Zhong, M., and Jang, M.: Light absorption coefficient measurement of SOA using a UV-Visible spectrometer
955 connected with an integrating sphere, *Atmospheric Environment*, 45, 4263-4271, 10.1016/j.atmosenv.2011.04.082,
956 2011.
957 Zhu, C. S., Cao, J. J., Huang, R. J., Shen, Z. X., Wang, Q. Y., and Zhang, N. N.: Light absorption properties of
958 brown carbon over the southeastern Tibetan Plateau, *Science of the Total Environment*, 625, 246-251,
959 10.1016/j.scitotenv.2017.12.183, 2018.
960